nature chemistry

Article

https://doi.org/10.1038/s41557-023-01400-0

A molecular-level mechanistic framework for interfacial proton-coupled electron transfer kinetics

In the format provided by the authors and unedited

Table of Contents:

1. Supplementary Notes

1.1 Supplementary Note 1: Detailed description of outer-sphere proton coupled electron transfer

A central focus of this work is to expose contrasts between inner-sphere, interfacial PCET (I-PCET) and outer-sphere PCET (OS-PCET). We include here a description of OS-PCET to provide context for the findings of the main text. The thermokinetic description of surface bound OS-PCET dates to 1980 to the work of Etienne Laviron who in a concurrent series of papers developed the trumpet plot analysis we used to quantify I-PCET rates. Derived from the work of Laviron[1] and others,[2–4] below are three sections outlining the 1) speciation, 2) thermodynamics, and 3) kinetics of OS-PCET processes.

Speciation: The four species that play a role in OS-PCET are commonly depicted in a square scheme (**Supplementary Figure 1**). In a square scheme horizontal movement between species reflects proton transfer and vertical movement reflects electron transfer (ET). The four species based on a general OS-PCET active molecule ("M") are: an oxidized deprotonated species, M (top left), a reduced deprotonated species, M/e$^-$ (bottom left), an oxidized protonated species, M/H$^+$ (top right), and a reduced protonated species M/e$^-$/H$^+$ (bottom right). Between these species there are five total reactions that can occur, two ET reactions, two PT reactions, as well as concerted proton electron transfer (CPET) direct from M to M/e$^-$/H$^+$. For the same PCET, the two ET and PT steps can be separated into two pathways one where ET precedes PT (ET_1PT_2) and one where PT precedes ET (PT_1ET_2). The reactions for ET_1PT_2 can be written as:

ET_1: $\mathrm{M} + \mathrm{e}^- \overset{E^0_{\mathrm{M}},\, k^0_{\mathrm{M}}}{\rightleftharpoons} \mathrm{M/e}^-$ $\qquad$ PT_2: $\mathrm{M/e}^- + \mathrm{H}^+ \overset{\mathrm{p}K_{\mathrm{a,M/e}^-}}{\rightleftharpoons} \mathrm{M/H}^+\mathrm{/e}^-$

PT_1ET_2 can be written as:

PT_1: $\mathrm{M} + \mathrm{H}^+ \overset{\mathrm{p}K_{\mathrm{a,M}}}{\rightleftharpoons} \mathrm{M/H}^+$ $\qquad$ ET_2: $\mathrm{M/H}^+ + \mathrm{e}^- \overset{E^0_{\mathrm{M/H}^+},\, k^0_{\mathrm{M/H}^+}}{\rightleftharpoons} \mathrm{M/e}^-\mathrm{/H}^+$

While CPET, in which electrons and protons transfer in a single step, can be written as:

CPET: $\mathrm{M} + \mathrm{e}^- + \mathrm{H}^+ \overset{E^0_{\mathrm{CPET}},\ k^0_{\mathrm{CPET}},\, \mathrm{p}K_{\mathrm{a,CPET}}}{\rightleftharpoons} \mathrm{M/e}^-\mathrm{/H}^+$

For the ET reactions E^0 is the standard potential while k^0 refers to the standard electron transfer rate constant of each reaction. For the PT reactions pK_a refers to the acid dissociation constants. In aqueous media the protonation steps are assumed to be in fast equilibrium,[4] as such we need not consider the rate constants of the PT reactions. CPET is generally not observed in aqueous media except for reactions where $\mathrm{p}K_{\mathrm{a,M}}$ and $\mathrm{p}K_{\mathrm{a,M/e}^-}$ differ significantly and in the presence of a high (>1 M) concentration of mid-pK_a buffering species.[4] (the CPET is included for completeness but is not considered further.) The reactivity motif of OS-PCET is quite different from I-PCET where barrierless ET from the external circuit to the electrode's delocalized band states forces ET and PT to occur exclusively as CPET and precludes supposed pseudo-M/H$^+$ or pseudo-M/e$^-$ states. This discrepancy in I-PCET speciation leads to significant differences in I-PCET thermochemical and kinetic behavior as a function of pH.

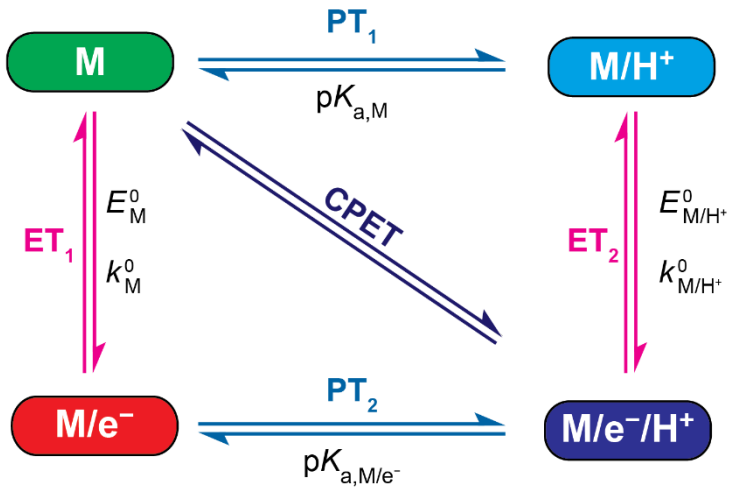

Supplementary Figure 1: Square scheme for generic OS-PCET reagent "M." Horizontal trajectories represent proton transfer while vertical trajectories represent electron transfer. Traversing from M to M/e$^-$/H$^+$ represents a full proton coupled electron transfer. The diagonal path represents concerted proton electron transfer (CPET)

Thermodynamics: For an OS-PCET reaction, the thermodynamically preferred state for "M" and the possible reactivity of said state are pH and potential dependent. The predominant state of "M" and the conditions that allow ET, PT, or CPET are summarized pictorially on a Pourbaix diagram in **Supplementary Figure 2**as a function of pH and potential. In this simulated Pourbaix diagram for "M" we defined the pK_a (vertical dashed lines) of each PT reaction to be 4 for p$K_{a,M/e^-}$ (red line) and 12 for p$K_{a,M}$ (blue line). The choice of p$K_{a,M/e^-}$ was to match the "zero-field" pK_a of GC-COOH (see main text) as an illustrative comparison. (The value of p$K_{a,M}$ of 12 was chosen to be far enough from 4 and 14 to easily illustrate the PCET behavior of "M.") The difference in the standard potentials of two PT reactions are linearly proportional to the difference in the PT reactions pK_a values. This is a result of Hess's Law, which requires the free energy of any pathway from M to M/e$^-$/H$^+$, whether ET$_1$PT$_2$, PT$_1$ET$_2$, or CPET, to be equal. Therefore:

$$\Delta G^0_{\mathrm{PT}_1} + \Delta G^0_{\mathrm{ET}_2} = \Delta G^0_{\mathrm{ET}_1} + \Delta \mathrm{G}^0_{\mathrm{PT}_2} \quad [S1]$$

$$-RT\ln\left(K_{a,M}\right) - \mathrm{F}E^0_{\mathrm{M/H^+}} = -\mathrm{F}E^0_{\mathrm{M}} - RT\ln\left(K_{a,M/e^-}\right) \quad [S2]$$

$$E^0_{\mathrm{M/H^+}} - E^0_{\mathrm{M}} = \frac{\ln(10)RT}{F}\left(\mathrm{p}K_{a,M} - \mathrm{p}K_{a,M/e^-}\right) \quad [S3]$$

Given the pK_a values as defined, $E^0_{\mathrm{M/H^+}}$ (higher dashed grey line) must be 0.47 V greater than E^0_{M} (lower grey dashed line). At potentials greater than E^0_{M} "M" is overwhelmingly oxidized while at potentials below $E^0_{\mathrm{M/H^+}}$ "M" is overwhelmingly reduced. At these potentials only PT occurs and so beyond these points the pH value at which PT occurs is potential independent. Similarly, at pH values below p$K_{a,M}$, "M" is overwhelmingly protonated while above p$K_{a,M/e^-}$ "M" is overwhelmingly deprotonated. At these pH values only ET occurs, while at more extreme pH levels the potential of ET is pH independent. PT and ET are coupled only between (or only very slightly beyond) these two pK_a and E^0 values.[1,3] The equilibrium potential of ET, E^{eq}, regardless of PT, is:

$$E^{\mathrm{eq}}(\mathrm{pH}) = E^0_{\mathrm{M}} + \frac{\ln(10)RT}{F}\log\left(\frac{1+10^{-\mathrm{pH}+\mathrm{p}K_{a,M/e^-}}}{1+10^{-\mathrm{pH}+\mathrm{p}K_{a,M}}}\right) \quad [S4]$$

A dark blue sigmoid ploting E^{eq} vs pH for the PCET of "M" using the defined pK_a values is shown in **Supplementary Figure 2**. This sigmoid clearly shows the potential independent regions as well as a Nernstian 59 mV pH^{-1} scaling between the two pK_a values. This description is general for any one-electron-one-proton outer-sphere PCET reaction. From **Equation [S4]** it is clear that the deviation in equilibrium potential for ET in OS-PCET

is simply the result of a shift in the protonation equilibria of the oxidized and reduced states. Moving to higher pH values shifts the protonation equilibria towards the deprotonated states of the species, increasing the electrochemical driving force needed to complete the overall PCET reaction.

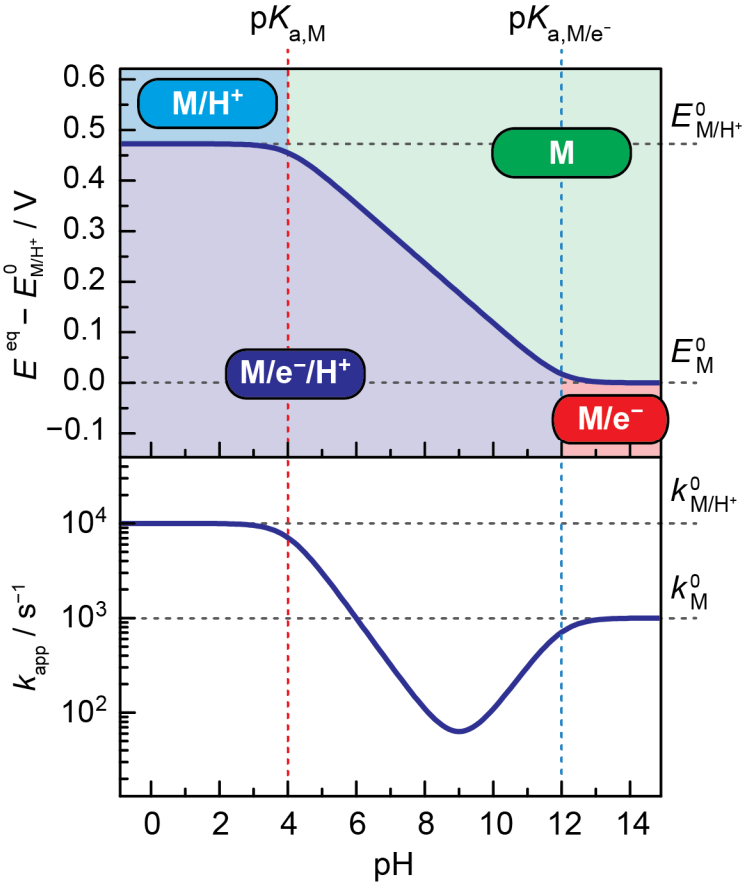

Supplementary Figure 2: Top: Pourbaix diagram for OS-PCET. Vertical dashed lines correspond to $pK_{a,M}$ (red) and $pK_{a,M/e^-}$ (blue), while the horizontal dashed lines correspond to the standard state reduction potentials for M and M/H^+. The purple sigmoid curve represents the equilibrium potential (E^{eq}) for ET as a function of pH following **Equation [S4].** The color–shaded regions represent the predominating species at each pH and potential, with pill-shaped labels for said species. Bottom: Inverted volcano plot representing the rate constant for OS-PCET as a function of pH with rate constants of $k^0_{M/H^+} = 10^4$ and $k^0_{M/H^+} = 10^3$. The "V"-shaped dependence of the apparent rate constant k_{app} on pH is shown in purple.

Kinetics: The kinetics of a surface-confined OS-PCET process as a function of pH are directly controlled by its pH-dependent thermodynamics. As the PT steps are assumed to be in rapid quasi-equilibrium in aqueous media,[S4] the overall rate for OS-PCET can be reduced to Butler-Volmer current potential dependencies for the sum of ET_1 (M to M/e^-) and ET_2 (M/H^+ to $M/e^-/H^+$) as given by the following equations:

$$j_{total} = k^0_M \left(\Gamma_{M/e^-} \exp\left(\frac{(1-\alpha_M)F(E-E^0_M)}{RT} \right) - \Gamma_M \exp\left(\frac{-\alpha_M F(E-E^0_M)}{RT} \right) \right)$$
$$+ k^0_{M/H^+} \left(\Gamma_{M/H^+/e^-} \exp\left(\frac{(1-\alpha_{M/H^+})F(E-E^0_{M/H^+})}{RT} \right) - \Gamma_{M/H^+} \exp\left(\frac{-\alpha_{M/H^+}F(E-E^0_{M/H^+})}{RT} \right) \right) \quad [S5]$$

Equation [S5] contains the currents of four half reactions, that is the oxidation and reduction each for ET_1 and ET_2. The first line corresponds to ET_1, electron transfer at the deprotonated species with rate constant k^0_M. These reactions are oxidation of M/e^- with surface coverage Γ_{M/e^-} and reduction of M with surface coverage Γ_M. The second line corresponds to electron transfer of the protonated species, ET_2, with rate constant k^0_{M/H^+}. These reactions are

oxidation of M/e⁻/H⁺ with surface coverage $\Gamma_{M/H^+/e^-}$ and reduction of M/H⁺ with surface coverage Γ_{M/H^+}. **Equation [S5]** can be simplified by considering the equilibrium constants of each protonation reaction such that:

$$K_{a,M/e^-} = \frac{\Gamma_{M/e^-} \times [H^+]}{\Gamma_{M/H^+/e^-}} \quad \text{where} \quad \Gamma_{M/e^-} = \Gamma_{M/H^+/e^-} \times 10^{pH - pK_{a,M/e^-}} \quad [S6]$$

$$K_{a,M} = \frac{\Gamma_M \times [H^+]}{\Gamma_{M/H^+}} \quad \text{where} \quad \Gamma_{M/H^+} = \Gamma_M \times 10^{-pH + pK_{a,M}} \quad [S7]$$

Substituting **Equations [S6] and [S7]** into **Equation [S5]** results in a current expression that relies only on the surface concentrations of the PCET end states, M and M/e⁻/H⁺:

$$j_{total}(E) = Fk_M^0 \left(\Gamma_{M/H^+/e^-} \times 10^{pH - pK_{a,M/e^-}} \times \exp\left(\frac{(1-\alpha_M)F\left(E - E_M^0\right)}{RT}\right) - \Gamma_M \exp\left(\frac{-\alpha_M F\left(E - E_M^0\right)}{RT}\right)\right)$$
$$+ Fk_{M/H^+}^0 \left(\Gamma_{M/H^+/e^-} \exp\left(\frac{\left(1-\alpha_{M/H^+}\right)F\left(E - E_{M/H^+}^0\right)}{RT}\right) - \Gamma_M \times 10^{-pH + pK_{a,M}} \times \exp\left(\frac{-\alpha_{M/H^+} F\left(E - E_{M/H^+}^0\right)}{RT}\right)\right) \quad [S8]$$

The currents of the half reactions in **Equation [S8]** can be group by direction, that is anodic (j_{anod}) and cathodic (j_{cath}) terms, to define currents for the overall forward and reverse reactions:

$$j_{anod}(E) = F\Gamma_{M/H^+/e^-} \left(k_M^0 10^{pH - pK_{a,M/e^-}} \times \exp\left(\frac{(1-\alpha_M)F\left(E - E_M^0\right)}{RT}\right) + k_{M/H^+}^0 \exp\left(\frac{\left(1-\alpha_{M/H^+}\right)F\left(E - E_{M/H^+}^0\right)}{RT}\right)\right) \quad [S9a]$$

$$j_{cath}(E) = -F\Gamma_M \left(k_M^0 \times \exp\left(\frac{-\alpha_M F\left(E - E_M^0\right)}{RT}\right) + k_{M/H^+}^0 10^{-pH + pK_{a,M}} \times \exp\left(\frac{-\alpha_{M/H^+} F\left(E - E_{M/H^+}^0\right)}{RT}\right)\right) \quad [S9b]$$

OS-PCET is at equilibrium when the total current is zero and $|j_{anod}| = |j_{cath}|$. For a given pH the forward and reverse current will be equal when $E = E^{eq}$. The apparent rate constant, k_{app}(pH), can then be determined by rearrangement of **Equations [S9a]** and **[S9b]** at this potential:

$$k_{app}(pH) = \left| \frac{j_{anod}\left(E^{eq}(pH)\right)}{F\Gamma_{M/H^+/e^-}} \right| = \left| \frac{j_{cath}\left(E^{eq}(pH)\right)}{F\Gamma_M} \right| \quad [S10]$$

Solving the above equation with the assumption that α_{M/H^+} and α_M equal 0.5 leads to a general closed form expression for the k_{app}:[3]

$$k_{app}(pH) = \left(k_M^0 + k_{M/H^+}^0 10^{-pH + \frac{pK_{a,M} + pK_{a,M/e^-}}{2}} \right) \left(1 + 10^{-pH + pK_{a,M/e^-}}\right)^{-\frac{1}{2}} \left(1 + 10^{-pH + pK_{a,M}}\right)^{-\frac{1}{2}} \quad [S11]$$

Notably, the ½ order exponents in **Equation [S11]** arise from the assumption that α = ½. **Equation [S11]** has only one variable, pH, and four system-defined constants, k_M^0, k_{M/H^+}^0, $pK_{a,M}$, and $pK_{a,M/e^-}$ that can be used to determine the apparent rate constant for OS-PCET at any pH.

Equation [S11] is plotted as log(k_{app}) vs pH in **Supplementary Figure 2**, bottom, as an inverted volcano plot, showing "V"-shaped pH dependence. For this illustration we used the same values for $pK_{a,M/e^-}$ and $pK_{a,M}$ as above and chose values of 10^4 s^{-1} and 10^3 s^{-1} for k_{M/H^+}^0 and k_M^0 respectively for illustration. Aligning the Pourbaix diagram and inverse volcano plot clearly illustrates how the speciation of "M" affects the observed rate. At pH 0 and until around pH = $pK_{a,M}$ "M" is always protonated. Since PT has already occurred, the overall apparent rate constant is simply the rate constant for ET_2. Likewise, from pH 14 down to around pH = $pK_{a,M/e^-}$ "M" is always deprotonated. Here too, no PT occurs and the overall apparent rate constant is simply the rate constant for ET_1. Between $pK_{a,M/e^-}$ and $pK_{a,M}$ a "V"-shape is seen with slopes of ± 0.5 orders of magnitude in rate constant per pH. In this example the "V" reaches a minimum at pH 9; this is the pH_{min} where OS-PCET is slowest. The position of pH_{min}, specifically its deviation from pH 7 is a function the pK_a and k^0 values of the species involved. Plots of **Equation [S11]** for many relative values of k_M^0, k_{M/H^+}^0, $pK_{a,M}$, and $pK_{a,M/e^-}$ can be found in reference 5.

In order to understand the origin of the inverted volcano plot's "V" shape seen by plotting **Equation [S11]**, the total apparent rate constant k_{app}(pH) can be separated into rate equations for ET_1 and ET_2:

$$k_{app,ET1}(pH) = k^0_M\left(1 + 10^{-pH+pK_{a,M/e^-}}\right)^{-\frac{1}{2}}\left(1 + 10^{-pH+pK_{a,M}}\right)^{-\frac{1}{2}} \quad [S12]$$

$$k_{app,ET2}(pH) = k^0_{M/H^+}10^{-pH+\frac{pK_{a,M}+pK_{a,M/e^-}}{2}}\left(1 + 10^{-pH+pK_{a,M/e^-}}\right)^{-\frac{1}{2}}\left(1 + 10^{-pH+pK_{a,M}}\right)^{-\frac{1}{2}} \quad [S13]$$

These individual apparent rate constants are plotted in **Supplementary Figure 3** overlaying their sum as it appears in **Supplementary Figure 2** (dashed purple line). The contribution to k_{app}(pH) from ET_1PT_2, $k_{app,ET1}(pH)$, is plotted in orange and the contribution from PT_1ET_2, $k_{app,ET2}(pH)$, is plotted in green. At low pH, $k_{app,ET2}(pH)$ is far larger than $k_{app,ET1}(pH)$ and nearly constant at k^0_{M/H^+} until $pK_{a,M}$. Past $pK_{a,M}$, $\log(k_{app,ET2}(pH))$ descends at a rate of –0.5 decades per pH (due to the defined α value). Alternatively at high pH, $k_{app,ET1}$ is greater with a value of k^0_M until $pK_{a,M/e^-}$. Past $pK_{a,M/e^-}$ the value of $\log\left(k_{app,ET1}(pH)\right)$ descends toward low pH at a rate of 0.5 decades per pH. In this high pH regime ET_1PT_2 prevails, but slows as a pH decreases past $k_{app,ET1}(pH)$. It follows from **Equations [S12] and [S13]** that the change in PCET rates at intermediate pH values are simply a reflection in the change of equilibrium concentrations of each protonated and deprotonated species as a function of pH. In this vein, in the pH regime where PT occurs with ET, starting from pH = $pK_{a,M}$, PT_1ET_2 accounts for nearly the entire apparent rate constant for PCET but slows as a function of pH as the protonated species are disfavored. ET_1PT_2 can in theory occur, but is orders of magnitude slower than PT_1ET_2, whose rate increases with pH. PT_1ET_2 predominates until pH_{min}, the pH where k_{app} is slowest. It is at pH_{min} that the rate of ET_1PT_2 supersedes PT_1ET_2 and takes over as the primary PCET pathway until pH = $pK_{a,M/e^-}$ after which only ET occurs. This is the source of the "V"-shape of the apparent rate constant of OS-PCET, a change in PCET mechanism from an PT_1ET_2 pathway to an ET_1PT_2 pathway.

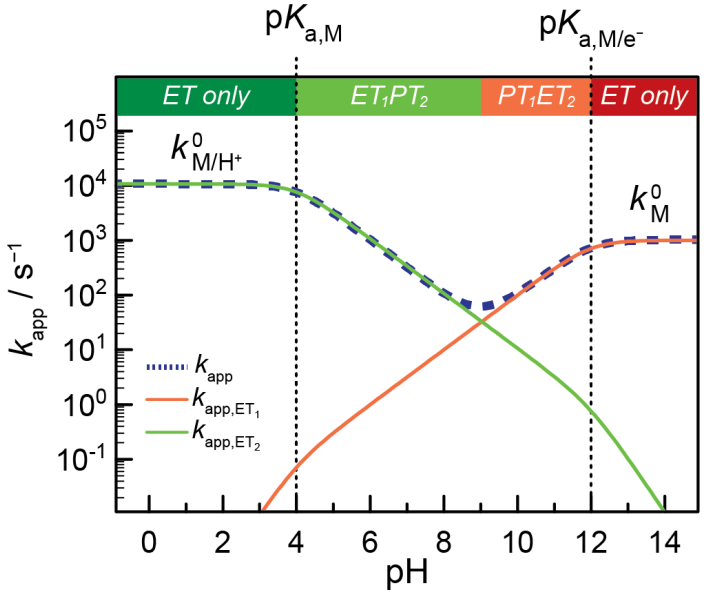

Supplementary Figure 3: OS-PCET inverted volcano plot for the same parameters as **Supplementary Figure 2**. The plot shows the contributions of the two pathways, PT_1ET_2 (green) and ET_1PT_2 (orange) to the overall apparent rate constant for OS-PCET in dashed purple. The predominate pathway is labeled above. At pH values more extreme than either pK_a only ET occurs, either because "M" has already been protonated at low pH or at high pH where protonation is highly disfavored. Deviation in k_{app} from the predominating process is seen only near pH 9 where the two processes display comparable rates. It is here that no pathway is overwhelmingly predominant and the otherwise predominant pathway shifts from PT_1ET_2 at low pH to ET_1PT_2 at high pH.

1.2 Supplementary Note 2: Detailed derivation of Equation 11 in the main text and a discussion of the equivalence of a "one-step" or "pre-association" reaction sequence

Surface I-PCET can be viewed as proceeding through a single elementary CPET step or via a three step sequence consisting of i) pre-association of the surface site and proton donor, ii) elementary CPET, and iii) dissociation of a successor complex of the protonated surface site and the conjugate proton acceptor. However, as noted in the main text, both the "one-step" and "pre-association" mechanisms result in equivalent expressions for the dependence of I-PCET rate on pH. In fact, after minor mathematical manipulation, the expression for the pre-association mechanism collapses to that of the single-step mechanism. In this section we will first show the equivalence of the one-step and pre-association mechanism before arriving at an expression equivalent to **Main Text Equation [11].** Our description of I-PCET begins with the two reactions, one where hydronium acts the proton donor and water as its conjugate acceptor and another where water acts as the proton donor and hydroxide as the proton acceptor to the carboxylate of GC-COOH as in the text. The one-step and pre-association mechanisms can be described in the following ways.

One-step:

$$\text{GC-COO}^- + \text{H}_3\text{O}^+ \underset{-\text{e}^-}{\overset{\text{e}^-, k_\text{a}^0, E_\text{a}^0}{\rightleftharpoons}} \text{e}^-/\text{GC-COOH} + \text{H}_2\text{O} \qquad \text{[S1a]}$$

$$\text{GC-COO}^- + \text{H}_2\text{O} \underset{-\text{e}^-}{\overset{\text{e}^-, k_\text{b}^0, E_\text{b}^0}{\rightleftharpoons}} \text{e}^-/\text{GC-COOH} + \text{OH}^- \qquad \text{[S1b]}$$

With pre-association:

$$\text{GC-COO}^- + \text{H}_3\text{O}^+ \overset{K_{1\text{a}}}{\rightleftharpoons} [\text{Ox}\cdot\cdot\text{H}_3\text{O}^+] \underset{-\text{e}^-}{\overset{\text{e}^-, k_\text{a}^{0,\text{el}}, E_\text{a}^{0,\text{el}}}{\rightleftharpoons}} [\text{RedH}\cdot\cdot\text{H}_2\text{O}] \overset{K_{2\text{a}}}{\rightleftharpoons} \text{e}^-/\text{GC-COOH} + \text{H}_2\text{O} \qquad \text{[S2a]}$$

$$\text{GC-COO}^- + \text{H}_2\text{O} \overset{K_{1\text{b}}}{\rightleftharpoons} [\text{Ox}\cdot\cdot\text{H}_2\text{O}] \underset{-\text{e}^-}{\overset{\text{e}^-, k_\text{b}^{0,\text{el}}, E_\text{b}^{0,\text{el}}}{\rightleftharpoons}} [\text{RedH}\cdot\cdot\text{OH}^-] \overset{K_{2\text{b}}}{\rightleftharpoons} \text{e}^-/\text{GC-COOH} + \text{OH}^- \qquad \text{[S2b]}$$

Where **Reaction [S1a]** and **Reaction [S2a]** are equivalent expressions for the overall "acid reaction," predominating at low pH while **Reaction [S1b]** and **Reaction [S2b]** are equivalent expressions for the overall "base reaction" predominating at high pH. Below, GC-COO$^-$ is referred to as "Ox," and GC-COOH as "RedH," while "e$^-$" represents an additional electron delocalized in the band states of the GC-COOH electrode. In all subsequent equations, the subscript "a" refers to the acid reaction and "b" to the base reaction. In **Reaction [S1a]**, k_a^0 and E_a^0 are the standard rate constant and standard state equilibrium potential, respectively, for the acid reaction. Likewise, for **Reaction [S1b]**, k_b^0 and E_b^0 are the standard rate constant and standard state equilibrium potentials, respectively, for base reaction. In **Reaction [S2a]**, $k_\text{a}^{0,\text{el}}$ and $E_\text{a}^{0,\text{el}}$ are respectively the standard rate constant and standard state equilibrium potential of the *elementary concerted* proton-electron transfer step to form the successor complex comprised of GC-COOH and a water molecule as the proton acceptor, [RedH$\cdot\cdot$H$_2$O]. $K_{1\text{a}}$ is the equilibrium constant for forming the acid reaction's precursor complex of GC-COO$^-$ and a hydronium ion proton donor, [Ox$\cdot\cdot$H$_3$O$^+$]. $K_{2\text{a}}$ is the equilibrium constant for splititng the successor complex into its constituent parts following CPET. In the base reaction, **Reaction [S2b]**, the symbols have the same meaning, but for the reaction where the precursor complex contains GC-COO$^-$ and a water molecule as the proton donor, [Ox$\cdot\cdot$H$_2$O], and the successor complex contains GC-COOH and a hydroxide ion as the proton acceptor, [RedH$\cdot\cdot$OH$^-$]. In both the acid and base reactions, standard state refers to the conditions where the surface coverage of RedH and Ox are equal and all proton donors and acceptors have an activity of 1. For the acid reaction this is at pH 0 and the base reaction this is at pH 14. To arrive at a simple expression for the dependence of the apparent rate constant for I-PCET on pH we will follow four steps:

1) Defining the potential dependence of the elementary CPET rates by a linear free energy relation.
2) Incorporating the equilibria of precursor complex formation and successor complex fragmentation.
3) Accounting for implicit equilibrium potential dependence of I-PCET using the Nernst equation.
4) Extracting apparent rate constants as the sum of the pH-dependent contributions of the acid and base reactions.

1) *Defining the potential dependence of the elementary CPET rates by a linear free energy relation.*
First, we define a linear free energy relation (LFER) for the I-PCET reactions. As noted in the Main Text the LFERs we define for the acid and base reactions are mathematically identical to those of a Butler-Volmer formalism or Brønsted rate law, however, are distinct in that they use current to measure the rate of proton transfer. These LFERs are defined as the elementary CPET reactions between either the initial and final states for the one-step sequence or the precursor and successor complexes for the pre-association sequence for both the acid and base reactions. The current-potential relationships can be defined for the "one-step" sequence as:

$$j_{\mathrm{a}}=Fk_{\mathrm{a}}^{0}\left(\Gamma_{\mathrm{RedH}}\times \mathrm{e}^{\frac{(1-\alpha_{\mathrm{a}})F}{RT}\left(E-E_{\mathrm{a}}^{0}\right)}-\Gamma_{\mathrm{Ox}}\times \mathrm{e}^{\frac{-\alpha_{\mathrm{a}}F}{RT}\left(E-E_{\mathrm{a}}^{0}\right)}\right) \quad [\mathrm{S14a}]$$

$$j_{\mathrm{b}}=Fk_{\mathrm{b}}^{0}\left(\Gamma_{\mathrm{RedH}}\times \mathrm{e}^{\frac{(1-\alpha_{\mathrm{b}})F}{RT}\left(E-E_{\mathrm{b}}^{0}\right)}-\Gamma_{\mathrm{Ox}}\times \mathrm{e}^{\frac{-\alpha_{\mathrm{b}}F}{RT}\left(E-E_{\mathrm{b}}^{0}\right)}\right) \quad [\mathrm{S14b}]$$

Where the Γ terms refer to the surface concentration of GC-COOH and GC-COO$^-$ and the rate constants are referenced to the overall reaction. For the pre-association sequence, the current dependence for the potential dependent elementary CPET step is:

$$j_{\mathrm{a}}=Fk_{\mathrm{a}}^{0,\mathrm{el}}\left(\Gamma_{\mathrm{RedH\cdot\cdot H_2O}}\times \mathrm{e}^{\frac{(1-\alpha_{\mathrm{a}})F}{RT}\left(E-E_{\mathrm{a}}^{0,\mathrm{el}}\right)}-\Gamma_{\mathrm{Ox\cdot\cdot H_3O^+}}\times \mathrm{e}^{\frac{-\alpha_{\mathrm{a}}F}{RT}\left(E-E_{\mathrm{a}}^{0,\mathrm{el}}\right)}\right) \quad [\mathrm{S15a}]$$

$$j_{\mathrm{b}}=Fk_{\mathrm{b}}^{0,\mathrm{el}}\left(\Gamma_{\mathrm{RedH\cdot\cdot OH^-}}\times \mathrm{e}^{\frac{(1-\alpha_{\mathrm{b}})F}{RT}\left(E-E_{\mathrm{b}}^{0,\mathrm{el}}\right)}-\Gamma_{\mathrm{Ox\cdot\cdot H_2O}}\times \mathrm{e}^{\frac{-\alpha_{\mathrm{b}}F}{RT}\left(E-E_{\mathrm{b}}^{0,\mathrm{el}}\right)}\right) \quad [\mathrm{S15b}]$$

Where the Γ terms refer to the surface concentration of each subscripted CPET precursor and successor complexes, while α_{a} and α_{b} refer to the charge transfer coefficient of the acid and base reactions, respectively. Below, we will show that with slight manipulation, the expressions in **Equations [S14a]** and **[S14b]** are equivalent to **Equations [S15a]** and **[S15b]**.

2) *Incorporating the association and dissociation equilibria to form the precursor/successor complexes*
While rigorously capturing the kinetics of the elementary CPET steps, the rate constants, surface concentrations, and potentials is **Equations [S15a] and [S15b]** cannot easily be related to measurable quantities. To address this, these equations can be translated into terms that incorporate measured potentials and quantifiable surface coverages. To do so, the CPET active surface complexes can be related to the starting and final state surface species and the activities of the solution proton donors and acceptors by the following relations:

$$\Gamma_{\mathrm{Ox\cdot\cdot H_3O^+}}=K_{1\mathrm{a}}\Gamma_{\mathrm{Ox}}a_{\mathrm{H_3O^+}} \qquad K_{1\mathrm{a}}=\frac{\Gamma_{\mathrm{Ox\cdot\cdot H_3O^+}}}{\Gamma_{\mathrm{Ox}}\times a_{\mathrm{H_3O^+}}} \quad [\mathrm{S16a}]$$

$$\Gamma_{\mathrm{RedH\cdot\cdot H_2O}}=\frac{1}{K_{2\mathrm{a}}}\Gamma_{\mathrm{RedH}}a_{\mathrm{H_2O}} \qquad K_{2\mathrm{a}}=\frac{\Gamma_{\mathrm{RedH}}\times a_{\mathrm{H_2O}}}{\Gamma_{\mathrm{RedH\cdot\cdot H_2O}}} \quad [\mathrm{S16b}]$$

$$\Gamma_{\mathrm{Ox\cdot\cdot H_2O}}=K_{1\mathrm{b}}\Gamma_{\mathrm{Ox}}a_{\mathrm{H_2O}} \qquad K_{1\mathrm{b}}=\frac{\Gamma_{\mathrm{Ox\cdot\cdot H_2O}}}{\Gamma_{\mathrm{Ox}}\times a_{\mathrm{H_2O}}} \quad [\mathrm{S16c}]$$

$$\Gamma_{\mathrm{RedH\cdot\cdot OH^-}}=\frac{1}{K_{2\mathrm{b}}}\Gamma_{\mathrm{RedH}}a_{\mathrm{OH^-}} \qquad K_{2\mathrm{b}}=\frac{\Gamma_{\mathrm{RedH}}\times a_{\mathrm{OH^-}}}{\Gamma_{\mathrm{RedH\cdot\cdot OH^-}}} \quad [\mathrm{S16d}]$$

Γ_{Ox} and Γ_{RedH} are the surface concentrations of uncomplexed GC-COO$^-$ and GC-COOH surface species respectively. The *a* terms refer to the solution activity of their subscripted species, with $a_{\mathrm{H_2O}}$ defined as 1.

The free energy of each overall PCET reaction is the sum of i) the free energy of forming the precursor complex from GC-COO$^-$ and a proton donor, ii) the free energy of the CPET reaction, and iii) the free energy of fragmenting the successor complex into GC-COOH and the proton acceptor.

$$\Delta G_{\mathrm{a}}^{0}=\Delta G_{\mathrm{a}}^{1}+\Delta G_{\mathrm{a}}^{0,\mathrm{el}}+\Delta G_{\mathrm{a}}^{2} \quad [\mathrm{S17a}]$$

$$\Delta G_{\mathrm{b}}^{0}=\Delta G_{\mathrm{b}}^{1}+\Delta G_{\mathrm{b}}^{0,\mathrm{el}}+\Delta G_{\mathrm{b}}^{2} \quad [\mathrm{S17b}]$$

Where $\Delta G_{\mathrm{a}}^{0}$and $\Delta G_{\mathrm{b}}^{0}$ are the overall free energies of the acid and base reaction respectively. Each ΔG^{1} term refers to the free energy of appropriate encounter complex formation, $\Delta G^{0,\mathrm{el}}$ to the free energy of the CPET within the encounter complex, and ΔG^{2} to encounter complex fragmentation. $\Delta G_{\mathrm{a}}^{0}$ and $\Delta G_{\mathrm{b}}^{0}$ can be redefined as potentials as follows:

$$-FE_{\mathrm{a}}^{0} = -\mathrm{RT}\ln(K_{1\mathrm{a}}) + -FE_{\mathrm{a}}^{0,\mathrm{el}} + -RT\ln(K_{2\mathrm{a}}) \quad \text{[S18a]}$$
$$-FE_{\mathrm{b}}^{0} = -\mathrm{RT}\ln(K_{1\mathrm{b}}) + -FE_{\mathrm{b}}^{0,\mathrm{el}} + -RT\ln(K_{2\mathrm{b}}) \quad \text{[S18b]}$$

Where E_{a}^{0} and E_{b}^{0} are each reaction's overall apparent standard state potential. Again, by Hess's law, the standard potential of the one-step (**Reactions [S1]**) and pre-association mechanisms (**Reactions [S2]**) must be equivalent. Simplifying **Equations [S18]** yields:

$$E_{\mathrm{a}}^{0,\mathrm{el}} = E_{\mathrm{a}}^{0} - \frac{RT}{F}\ln(K_{1\mathrm{a}}K_{2\mathrm{a}}) \quad \text{[S19a]}$$
$$E_{\mathrm{b}}^{0,\mathrm{el}} = E_{\mathrm{b}}^{0} - \frac{RT}{F}\ln(K_{1\mathrm{b}}K_{2\mathrm{b}}) \quad \text{[S19b]}$$

By substituting **Equations [S16]** and **Equations [S19]** into **Equations [S15]** we arrive at rate-potential expressions in terms of the initial and final end states, GC-COOH and GC-COO^{-} while utilizing the potentials of the overall reaction and only measurable quantities. These substitutions yield the following rate expression:

$$j_{\mathrm{a}} = Fk_{\mathrm{a}}^{0,\mathrm{el}}\left(\frac{1}{K_{2\mathrm{a}}}\Gamma_{\mathrm{RedH}}a_{\mathrm{H_2O}} \times \mathrm{e}^{\frac{(1-\alpha_{\mathrm{a}})F}{\mathrm{RT}}\left(E-\left(E_{\mathrm{a}}^{0}-\frac{RT}{F}\ln(K_{1\mathrm{a}}K_{2\mathrm{a}})\right)\right)} - K_{1\mathrm{a}}\Gamma_{\mathrm{Ox}}a_{\mathrm{H_3O^+}} \times \mathrm{e}^{\frac{-\alpha_{\mathrm{a}}F}{\mathrm{RT}}\left(E-\left(E_{\mathrm{a}}^{0}-\frac{RT}{F}\ln(K_{1\mathrm{a}}K_{2\mathrm{a}})\right)\right)}\right) \quad \text{[S20a]}$$
$$j_{\mathrm{b}} = Fk_{\mathrm{b}}^{0,\mathrm{el}}\left(\frac{1}{K_{2\mathrm{b}}}\Gamma_{\mathrm{RedH}}a_{\mathrm{OH^-}} \times \mathrm{e}^{\frac{(1-\alpha_{\mathrm{b}})F}{\mathrm{RT}}\left(E-\left(E_{\mathrm{b}}^{0}-\frac{RT}{F}\ln(K_{1\mathrm{b}}K_{2\mathrm{b}})\right)\right)} - K_{1\mathrm{b}}\Gamma_{\mathrm{Ox}}a_{\mathrm{H_2O}} \times \mathrm{e}^{\frac{-\alpha_{\mathrm{b}}F}{\mathrm{RT}}\left(E-\left(E_{\mathrm{b}}^{0}-\frac{RT}{F}\ln(K_{1\mathrm{b}}K_{2\mathrm{b}})\right)\right)}\right) \quad \text{[S20b]}$$

Distributing once to separate pre-association constants in the exponent:

$$j_{\mathrm{a}} = Fk_{\mathrm{a}}^{0,\mathrm{el}}\left(\frac{1}{K_{2\mathrm{a}}}\Gamma_{\mathrm{RedH}}a_{\mathrm{H_2O}} \times \mathrm{e}^{\frac{(1-\alpha_{\mathrm{a}})F}{RT}(E-E_{\mathrm{a}}^{0})+(1-\alpha_{\mathrm{a}})\ln(K_{1\mathrm{a}}K_{2\mathrm{a}})} - K_{1\mathrm{a}}\Gamma_{\mathrm{Ox}}a_{\mathrm{H_3O^+}} \times \mathrm{e}^{\frac{-\alpha_{\mathrm{a}}F}{RT}(E-E_{\mathrm{a}}^{0})+(-\alpha_{\mathrm{a}})\ln(K_{1\mathrm{a}}K_{2\mathrm{a}})}\right) \quad \text{[S21a]}$$
$$j_{\mathrm{b}} = Fk_{\mathrm{b}}^{0,\mathrm{el}}\left(\frac{1}{K_{2\mathrm{b}}}\Gamma_{\mathrm{RedH}}a_{\mathrm{OH^-}} \times \mathrm{e}^{\frac{(1-\alpha_{\mathrm{b}})F}{RT}(E-E_{\mathrm{b}}^{0})+(1-\alpha_{\mathrm{b}})\ln(K_{1\mathrm{b}}K_{2\mathrm{b}})} - K_{1\mathrm{b}}\Gamma_{\mathrm{Ox}}a_{\mathrm{H_2O}} \times \mathrm{e}^{\frac{-\alpha_{\mathrm{b}}F}{RT}(E-E_{\mathrm{b}}^{0})+(-\alpha_{\mathrm{b}})\ln(K_{1\mathrm{b}}K_{2\mathrm{b}})}\right) \quad \text{[S21b]}$$

Distributing again to pull the pre-association terms out of the exponent:

$$j_{\mathrm{a}} = Fk_{\mathrm{a}}^{0,\mathrm{el}}\left(\frac{1}{K_{2\mathrm{a}}}\Gamma_{\mathrm{RedH}}a_{\mathrm{H_2O}}(K_{1\mathrm{a}}K_{2\mathrm{a}})^{(1-\alpha_a)}\mathrm{e}^{\frac{(1-\alpha_{\mathrm{a}})F}{RT}(E-E_{\mathrm{a}}^{0})} - K_{1\mathrm{a}}\Gamma_{\mathrm{Ox}}a_{\mathrm{H_3O^+}}(K_{1\mathrm{a}}K_{2\mathrm{a}})^{(-\alpha_{\mathrm{a}})}\mathrm{e}^{\frac{-\alpha_{\mathrm{a}}F}{RT}(E-E_{\mathrm{a}}^{0})}\right) \quad \text{[S22a]}$$
$$j_{\mathrm{b}} = Fk_{\mathrm{b}}^{0,\mathrm{el}}\left(\frac{1}{K_{2\mathrm{b}}}\Gamma_{\mathrm{RedH}}a_{\mathrm{OH^-}}(K_{1\mathrm{b}}K_{2\mathrm{b}})^{(1-\alpha_{\mathrm{b}})}\mathrm{e}^{\frac{(1-\alpha_{\mathrm{b}})F}{RT}(E-E_{\mathrm{b}}^{0})} - K_{1\mathrm{b}}\Gamma_{\mathrm{Ox}}a_{\mathrm{H_2O}}(K_{1\mathrm{b}}K_{2\mathrm{b}})^{(-\alpha_{\mathrm{b}})}\mathrm{e}^{\frac{-\alpha_{\mathrm{b}}F}{RT}(E-E_{\mathrm{b}}^{0})}\right) \quad \text{[S22b]}$$

Rearranging a third time to combine pre-association terms due to a) changing reference surface concentrations to Γ_{Ox} and Γ_{RedH} and b) changing reference potentials to equilibrium potentials from standard state potentials yields:

$$j_{\mathrm{a}} = Fk_{\mathrm{a}}^{0,\mathrm{el}}\left((K_{2a})^{-\alpha_a}(K_{1\mathrm{a}})^{(1-\alpha_a)}\Gamma_{\mathrm{RedH}}a_{\mathrm{H_2O}}\mathrm{e}^{\frac{(1-\alpha_{\mathrm{a}})F}{RT}(E-E_{\mathrm{a}}^{0})} - (K_{2a})^{-\alpha_a}(K_{1\mathrm{a}})^{(1-\alpha_a)}\Gamma_{\mathrm{Ox}}a_{\mathrm{H_3O^+}}\mathrm{e}^{\frac{-\alpha_{\mathrm{a}}F}{RT}(E-E_{\mathrm{a}}^{0})}\right) \quad \text{[S23a]}$$
$$j_{\mathrm{b}} = Fk_{\mathrm{b}}^{0,\mathrm{el}}\left((K_{2\mathrm{b}})^{-\alpha_{\mathrm{b}}}(K_{1\mathrm{b}})^{(1-\alpha_{\mathrm{b}})}\Gamma_{\mathrm{RedH}}a_{\mathrm{OH^-}}\mathrm{e}^{\frac{(1-\alpha_{\mathrm{b}})F}{RT}(E-E_{\mathrm{b}}^{0})} - (K_{2\mathrm{b}})^{-\alpha_{\mathrm{b}}}(K_{1\mathrm{b}})^{(1-\alpha_{\mathrm{b}})}\Gamma_{\mathrm{Ox}}a_{\mathrm{H_2O}}\mathrm{e}^{\frac{-\alpha_{\mathrm{b}}F}{RT}(E-E_{\mathrm{b}}^{0})}\right) \quad \text{[S23b]}$$

In both the acid and base reactions each constituent half reaction, in the oxidative and reductive directions, have the same pre-exponential factors comprised of the equilibrium constants for forming the precursor complexes and fragmenting the successor complexes. In light of this we can redefine a bimolecular, overall rate constants $k_{\mathrm{a}}^{0,\mathrm{bim}}$and $k_{\mathrm{b}}^{0,\mathrm{bim}}$ for I-PCET such that:

$$k_{\mathrm{a}}^{0,\mathrm{bim}} = k_{\mathrm{a}}^{0,\mathrm{el}}(K_{2a})^{-\alpha_a}(K_{1\mathrm{a}})^{(1-\alpha_a)} \quad [S24a]$$
$$k_{\mathrm{b}}^{0,\mathrm{bim}} = k_{\mathrm{b}}^{0,\mathrm{el}}(K_{2\mathrm{b}})^{-\alpha_\mathrm{b}}(K_{1\mathrm{b}})^{(1-\alpha_\mathrm{b})} \quad [S24b]$$

Substituting **Equations [S23]** into **Equations [S22]** yields:

$$j_{\mathrm{a}} = Fk_{\mathrm{a}}^{0,\mathrm{bim}}\left(\Gamma_{\mathrm{RedH}}a_{\mathrm{H_2O}}\mathrm{e}^{\frac{(1-\alpha_\mathrm{a})F}{RT}(E-E_{\mathrm{a}}^{0})} - \Gamma_{\mathrm{Ox}}a_{\mathrm{H_3O^+}}\mathrm{e}^{\frac{-\alpha_\mathrm{a}F}{RT}(E-E_{\mathrm{a}}^{0})}\right) \quad [S25a]$$
$$j_{\mathrm{b}} = Fk_{\mathrm{b}}^{0,\mathrm{bim}}\left(\Gamma_{\mathrm{RedH}}a_{\mathrm{OH^-}}\mathrm{e}^{\frac{(1-\alpha_\mathrm{b})F}{RT}(E-E_{\mathrm{b}}^{0})} - \Gamma_{\mathrm{Ox}}a_{\mathrm{H_2O}}\mathrm{e}^{\frac{-\alpha_\mathrm{b}F}{RT}(E-E_{\mathrm{b}}^{0})}\right) \quad [S25b]$$

Equation [S25a] and **Equation [25b]** correspond to LFER rate equations for the acid and base reaction respectively corresponding to measurable potentials and surface coverages. The two equations appear very similar to **Equation [S15a]** and **Equation [15b]** but with *apparent* standard potentials and rate constants that explicitly account for, but obviate the need to measure, the pre-association constants for each reaction. Furthermore, save for the label of the acid and base reactions' rate constant, **Equation [S25a]** and **Equation [S25b]** correspond exactly to **Main Text Equation [2a]** and **Main Text Equation [2b].** As a result $k_{\mathrm{a}}^{0,\mathrm{bim}}$ can be taken as equivalent to k_{a}^{0}, and $k_{\mathrm{b}}^{0,\mathrm{bim}}$ as equivalent to k_{b}^{0}. Substituting the bimolecular rate constant labels for the overall rate constant yields:

$$j_{\mathrm{a}} = Fk_{\mathrm{a}}^{0}\left(\Gamma_{\mathrm{RedH}}a_{\mathrm{H_2O}}\mathrm{e}^{\frac{(1-\alpha_\mathrm{a})F}{RT}(E-E_{\mathrm{a}}^{0})} - \Gamma_{\mathrm{Ox}}a_{\mathrm{H_3O^+}}\mathrm{e}^{\frac{-\alpha_\mathrm{a}F}{RT}(E-E_{\mathrm{a}}^{0})}\right) \quad [S26a]$$
$$j_{\mathrm{b}} = Fk_{\mathrm{b}}^{0}\left(\Gamma_{\mathrm{RedH}}a_{\mathrm{OH^-}}\mathrm{e}^{\frac{(1-\alpha_\mathrm{b})F}{RT}(E-E_{\mathrm{b}}^{0})} - \Gamma_{\mathrm{Ox}}a_{\mathrm{H_2O}}\mathrm{e}^{\frac{-\alpha_\mathrm{b}F}{RT}(E-E_{\mathrm{b}}^{0})}\right) \quad [S26b]$$

Equations [S26a] and **[S26b]** derived from the pre-association sequence correspond *exactly* to **Equations [S14a]** and **[S14b]** derived from the simpler one-step sequence. This analysis highlights that both the one-step and pre-association models give rise to the same mathematical form and are, thus, kinetically indistinguishable in our study.

3) *Accounting for implicit potential dependence using Nernstian relation*.
In order to understand I-PCET kinetics away from standard state, pH 0 for the acid and pH 14 base reaction, we can define the current for each reaction to their respective equilibrium potentials (E^{eq}) for any given pH. This can be done using a Nernstian potential dependence on pH:

$$E_{\mathrm{a}}^{\mathrm{eq}}(\mathrm{pH}) = E_{\mathrm{a}}^{0} - \frac{RT}{F}\ln\left(\frac{a_{\mathrm{H_2O}}}{a_{\mathrm{H_3O^+}}}\right) = E_{\mathrm{a}}^{0} - \frac{RT\ln(10)}{F}\mathrm{pH} \quad [S27a]$$
$$E_{\mathrm{b}}^{\mathrm{eq}}(\mathrm{pH}) = E_{\mathrm{b}}^{0} - \frac{RT}{F}\ln\left(\frac{a_{\mathrm{OH^-}}}{a_{\mathrm{H_2O}}}\right) = E_{\mathrm{b}}^{0} - \frac{RT\ln(10)}{F}(\mathrm{pH} - \mathrm{p}K_{\mathrm{w}}) \quad [S27b]$$

Subtracting the reactants and products of **Reaction [S1a]** from **Reaction [S1b]** reveals that they differ only by the dissociation of water:

$$2\ \mathrm{H_2O} \overset{K_{\mathrm{w}}}{\rightleftharpoons} \mathrm{H_3O^+} + \mathrm{OH^-} \quad [S3]$$

Such that:

$$\Delta G_{\mathrm{b}}^{0} - \Delta G_{\mathrm{a}}^{0} = -FE_{\mathrm{b}}^{0} - (-FE_{\mathrm{a}}^{0}) = -RT\ln(K_w) \quad [S28]$$
$$E_{\mathrm{b}}^{0} = E_{\mathrm{a}}^{0} + \frac{RT}{F}\ln(K_w) = E_{\mathrm{a}}^{0} - \frac{RT\ln(10)}{F}\mathrm{p}K_w \quad [S29]$$

Where K_{W} is the auto-dissociation constant of water. Substituting **Equation [S29]** into **Equation [S27b]** yields:

$$E_{\mathrm{b}}^{\mathrm{eq}}(\mathrm{pH}) = E_{\mathrm{a}}^{0} - \frac{RT\ln(10)}{F}\mathrm{p}K_w - \frac{RT\ln(10)}{F}(\mathrm{pH} - \mathrm{p}K_{\mathrm{w}}) = E_{\mathrm{a}}^{0} - \frac{RT\ln(10)}{F}(\mathrm{pH}) \quad [S30]$$

Equation [S30] equates both **Equation [S27a]** and **Equation [S27b]** indicating that the equilibrium potentials for the acid and base reaction are equivalent:

$$E_{\mathrm{pH}}^{\mathrm{eq}} = E_{\mathrm{a}}^{\mathrm{eq}}(\mathrm{pH}) = E_{\mathrm{b}}^{\mathrm{eq}}(\mathrm{pH}) = E_{\mathrm{a}}^{0} - \frac{RT\ln(10)}{F}\mathrm{pH} = E_{\mathrm{b}}^{0} - \frac{RT\ln(10)}{F}(\mathrm{pH} - \mathrm{p}K_{\mathrm{w}}) \quad [S31]$$

Substituting **Equation [S31]** into **Equations [S25]** yields expressions referenced to equilibrium potentials:

$$j_{\mathrm{a}} = Fk_{\mathrm{a}}^{0}\left(\Gamma_{\mathrm{RedH}}a_{\mathrm{H_2O}}\mathrm{e}^{\frac{(1-\alpha_{\mathrm{a}})F}{\mathrm{RT}}\left(E-E_{\mathrm{pH}}^{\mathrm{eq}}-\frac{RT\ln(10)}{F}\mathrm{pH}\right)} - \Gamma_{\mathrm{Ox}}a_{\mathrm{H_3O^+}}\mathrm{e}^{\frac{-\alpha_{\mathrm{a}}F}{\mathrm{RT}}\left(E-E_{\mathrm{pH}}^{\mathrm{eq}}-\frac{RT\ln(10)}{F}\mathrm{pH}\right)}\right) \quad [S32a]$$

$$j_{\mathrm{b}} = Fk_{\mathrm{b}}^{0}\left(\Gamma_{\mathrm{RedH}}a_{\mathrm{OH^-}}\mathrm{e}^{\frac{(1-\alpha_{\mathrm{b}})F}{\mathrm{RT}}\left(E-E_{\mathrm{pH}}^{\mathrm{eq}}-\frac{RT\ln(10)}{F}(\mathrm{pH}-\mathrm{p}K_{\mathrm{w}})\right)} - \Gamma_{\mathrm{Ox}}a_{\mathrm{H_2O}}\mathrm{e}^{\frac{-\alpha_{\mathrm{b}}F}{\mathrm{RT}}\left(E-E_{\mathrm{pH}}^{\mathrm{eq}}-\frac{RT\ln(10)}{F}(\mathrm{pH}-\mathrm{p}K_{\mathrm{w}})\right)}\right) \quad [S32b]$$

Now we translate the solution proton donor and acceptor activities to pH terms, with $a_{\mathrm{H_2O}}$ taken as unity.

$$j_{\mathrm{a}} = Fk_{\mathrm{a}}^{0}\left(\Gamma_{\mathrm{RedH}}\mathrm{e}^{\frac{(1-\alpha_{\mathrm{a}})F}{RT}\left(E-E_{\mathrm{pH}}^{\mathrm{eq}}-\frac{RT\ln(10)}{F}\mathrm{pH}\right)} - \Gamma_{\mathrm{Ox}}10^{-\mathrm{pH}}\mathrm{e}^{\frac{-\alpha_{\mathrm{a}}F}{RT}\left(E-E_{\mathrm{pH}}^{\mathrm{eq}}-\frac{RT\ln(10)}{F}\mathrm{pH}\right)}\right) \quad [S33a]$$

$$j_{\mathrm{b}} = Fk_{\mathrm{b}}^{0}\left(\Gamma_{\mathrm{RedH}}10^{-(\mathrm{p}K_{\mathrm{w}}-\mathrm{pH})}\mathrm{e}^{\frac{(1-\alpha_{\mathrm{b}})F}{RT}\left(E-E_{\mathrm{pH}}^{\mathrm{eq}}-\frac{RT\ln(10)}{F}(\mathrm{pH}-\mathrm{p}K_{\mathrm{w}})\right)} - \Gamma_{\mathrm{Ox}}\mathrm{e}^{\frac{-\alpha_{\mathrm{b}}F}{RT}\left(E-E_{\mathrm{pH}}^{\mathrm{eq}}-\frac{RT\ln(10)}{F}(\mathrm{pH}-\mathrm{p}K_{\mathrm{w}})\right)}\right) \quad [S33b]$$

Now we distribute the exponents to separate out the pH terms from the potential terms:

$$j_{\mathrm{a}} = Fk_{\mathrm{a}}^{0}\left(\Gamma_{\mathrm{RedH}}\mathrm{e}^{\frac{(1-\alpha_{\mathrm{a}})F}{RT}\left(E-E_{\mathrm{pH}}^{\mathrm{eq}}\right)-(1-\alpha_{\mathrm{a}})\ln(10)\mathrm{pH}} - \Gamma_{\mathrm{Ox}}10^{-\mathrm{pH}}\mathrm{e}^{\frac{-\alpha_{\mathrm{a}}F}{RT}\left(E-E_{\mathrm{pH}}^{\mathrm{eq}}\right)-(-\alpha_{\mathrm{a}})\ln(10)\mathrm{pH}}\right) \quad [S34a]$$

$$j_{\mathrm{b}} = Fk_{\mathrm{b}}^{0}\left(\Gamma_{\mathrm{RedH}}10^{-(\mathrm{p}K_{\mathrm{w}}-\mathrm{pH})}\mathrm{e}^{\frac{(1-\alpha_{\mathrm{b}})F}{RT}\left(E-E_{\mathrm{pH}}^{\mathrm{eq}}\right)-(1-\alpha_{\mathrm{b}})\ln(10)(\mathrm{pH}-\mathrm{p}K_{\mathrm{w}})} - \Gamma_{\mathrm{Ox}}\mathrm{e}^{\frac{-\alpha_{\mathrm{b}}F}{RT}\left(E-E_{\mathrm{pH}}^{\mathrm{eq}}\right)-(-\alpha_{\mathrm{b}})\ln(10)(\mathrm{pH}-\mathrm{p}K_{\mathrm{w}})}\right) \quad [S34b]$$

Pulling the pH and pK_{w} terms outside of the exponent yields:

$$j_{\mathrm{a}} = Fk_{\mathrm{a}}^{0}\left(\Gamma_{\mathrm{RedH}}\left(10^{-(1-\alpha_{\mathrm{a}})\mathrm{pH}} \times \mathrm{e}^{\frac{(1-\alpha_{\mathrm{a}})F}{RT}\left(E-E_{\mathrm{pH}}^{\mathrm{eq}}\right)}\right) - \Gamma_{\mathrm{Ox}}\left(10^{-\mathrm{pH}}\right)\left(10^{\alpha_{\mathrm{a}}\mathrm{pH}}\right)\mathrm{e}^{\frac{-\alpha_{\mathrm{a}}F}{RT}\left(E-E_{\mathrm{pH}}^{\mathrm{eq}}\right)}\right) \quad [S35a]$$

$$j_{\mathrm{b}} = Fk_{\mathrm{b}}^{0}\left(\Gamma_{\mathrm{RedH}}\left(10^{-(\mathrm{p}K_{\mathrm{w}}-\mathrm{pH})}\right)\left(10^{-(1-\alpha_{\mathrm{b}})(\mathrm{pH}-\mathrm{p}K_{\mathrm{w}})}\mathrm{e}^{\frac{(1-\alpha_{\mathrm{b}})F}{RT}\left(E-E_{\mathrm{pH}}^{\mathrm{eq}}\right)}\right) - \Gamma_{\mathrm{Ox}}\left(10^{\alpha_{\mathrm{b}}(\mathrm{pH}-\mathrm{p}K_{\mathrm{w}})}\mathrm{e}^{\frac{-\alpha_{\mathrm{b}}F}{RT}\left(E-E_{\mathrm{pH}}^{\mathrm{eq}}\right)}\right)\right) \quad [S35b]$$

Combining the pH and pK_{w} terms yields two final rate expressions for the acid and base reaction:

$$j_{\mathrm{a}} = Fk_{\mathrm{a}}^{0}10^{-(1-\alpha_{\mathrm{a}})\mathrm{pH}}\left(\Gamma_{\mathrm{RedH}}\mathrm{e}^{\frac{(1-\alpha_{\mathrm{a}})F}{RT}\left(E-E_{\mathrm{pH}}^{\mathrm{eq}}\right)} - \Gamma_{\mathrm{Ox}}\mathrm{e}^{\frac{-\alpha_{\mathrm{a}}F}{RT}\left(E-E_{\mathrm{pH}}^{\mathrm{eq}}\right)}\right) \quad [S36a]$$

$$j_{\mathrm{b}} = Fk_{\mathrm{b}}^{0}10^{\alpha_{\mathrm{b}}(\mathrm{pH}-\mathrm{pK_w})}\left(\Gamma_{\mathrm{RedH}}\mathrm{e}^{\frac{(1-\alpha_{\mathrm{b}})F}{RT}\left(E-E_{\mathrm{pH}}^{\mathrm{eq}}\right)} - \Gamma_{\mathrm{Ox}}\mathrm{e}^{\frac{-\alpha_{\mathrm{b}}F}{RT}\left(E-E_{\mathrm{pH}}^{\mathrm{eq}}\right)}\right) \quad [S36b]$$

The current expressions in **Equations [S36]** are the same as **Main Text Equations [9a] and [9b].** The currents in **Equations [S36]** are referenced to observed rate constants and measured equilibrium potentials and are applicable for any pH.

4) Extracting apparent rate constants as the sum of the pH dependent contributions of acid and base reaction
Finally, an overall rate constant for I-PCET at GC-COOH can be found by calculating an apparent rate constant corresponding to the total current of all reactions occurring at a given $E_{\mathrm{pH}}^{\mathrm{eq}}$. For a given pH, when the anodic and cathodic currents are equal and opposite, the total current is zero and the reaction is at equilibrium. It is under these conditions that an apparent pH dependent rate constant can be extracted. The total current (j_{total}) for a given potential and pH is simply the sum of the acid and base reactions, **Equation [S37].**

$$j_{\text{total}} = j_{\text{a}} + j_{\text{b}} = Fk_{\text{a}}^{0}10^{-(1-\alpha_{\text{a}})\text{pH}}\left(\Gamma_{\text{RedH}}\text{e}^{\frac{(1-\alpha_{\text{a}})F}{RT}\left(E-E_{\text{pH}}^{\text{eq}}\right)} - \Gamma_{\text{Ox}}\text{e}^{\frac{-\alpha_{\text{a}}F}{RT}\left(E-E_{\text{pH}}^{\text{eq}}\right)}\right) + Fk_{\text{b}}^{0}10^{\alpha_{\text{b}}(\text{pH}-\text{p}K_{\text{w}})}\left(\Gamma_{\text{RedH}}\text{e}^{\frac{(1-\alpha_{\text{b}})F}{RT}\left(E-E_{\text{pH}}^{\text{eq}}\right)} - \Gamma_{\text{Ox}}\text{e}^{\frac{-\alpha_{\text{b}}F}{RT}\left(E-E_{\text{pH}}^{\text{eq}}\right)}\right) \quad \text{[S37]}$$

The terms in **Equation [S37]** and **Equations [S36]** are grouped by donor/acceptor couples, each with an anodic and cathodic half reaction. Alternatively, it is equally valid to group these terms by reaction direction, that is the acid and base cathodic half reactions and the acid and base anodic half reactions. First, we can rearrange the terms in **Equation [S37]** to get a new expression for j_{total} with this new grouping:

$$j_{\text{total}} = j_{\text{anod}} + j_{\text{cath}} = F\Gamma_{\text{RedH}}\left(k_{\text{a}}^{0}10^{-(1-\alpha_{\text{a}})\text{pH}}\text{e}^{\frac{(1-\alpha_{\text{a}})F}{RT}\left(E-E_{\text{pH}}^{\text{eq}}\right)} + k_{\text{b}}^{0}10^{\alpha_{\text{b}}(\text{pH}-\text{p}K_{\text{w}})}\text{e}^{\frac{(1-\alpha_{\text{b}})F}{RT}\left(E-E_{\text{pH}}^{\text{eq}}\right)}\right) - F\Gamma_{\text{Ox}}\left(k_{\text{a}}^{0}10^{-(1-\alpha_{\text{a}})\text{pH}}\text{e}^{\frac{-\alpha_{\text{a}}F}{RT}\left(E-E_{\text{pH}}^{\text{eq}}\right)} + k_{\text{b}}^{0}10^{\alpha_{\text{b}}(\text{pH}-\text{p}K_{\text{w}})}\text{e}^{\frac{-\alpha_{\text{b}}F}{RT}\left(E-E_{\text{pH}}^{\text{eq}}\right)}\right) \quad \text{[S38]}$$

In **Equation [S38]**, the top line refers to the reverse anodic current j_{anod} for GC-COOH (Γ_{RedH}) deprotonation by water (acid reaction) and hydroxide (base reaction), while the bottom line refers to the forward cathodic current j_{cath} for GC-COO$^-$ (Γ_{Ox}) protonation by hydronium (acid reaction) and water (base reaction).

$$j_{\text{anod}} = F\Gamma_{\text{RedH}}\left(k_{\text{a}}^{0}10^{-(1-\alpha_{\text{a}})\text{pH}}\text{e}^{\frac{(1-\alpha_{\text{a}})F}{RT}\left(E-E_{\text{pH}}^{\text{eq}}\right)} + k_{\text{b}}^{0}10^{\alpha_{\text{b}}(\text{pH}-\text{p}K_{\text{w}})}\text{e}^{\frac{(1-\alpha_{\text{b}})F}{RT}\left(E-E_{\text{pH}}^{\text{eq}}\right)}\right) \quad \text{[S39a]}$$

$$j_{\text{cath}} = -F\Gamma_{\text{Ox}}\left(k_{\text{a}}^{0}10^{-(1-\alpha_{\text{a}})\text{pH}}\text{e}^{\frac{-\alpha_{\text{a}}F}{RT}\left(E-E_{\text{pH}}^{\text{eq}}\right)} + k_{\text{b}}^{0}10^{\alpha_{\text{b}}(\text{pH}-\text{p}K_{\text{w}})}\text{e}^{\frac{-\alpha_{\text{b}}F}{RT}\left(E-E_{\text{pH}}^{\text{eq}}\right)}\right) \quad \text{[S39b]}$$

At a given pH condition, at the equilibrium potential where $E = E_{\text{pH}}^{\text{eq}}$ the forward and reverse currents are equal in magnitude by definition ($|j_{\text{anod}}| = |j_{\text{cath}}|$) and $j_{\text{total}} = 0$. We can define an apparent rate constant for I-PCET such that:

$$k_{\text{app}}(\text{pH}) = \left|\frac{j_{\text{anod}}\left(E_{\text{pH}}^{\text{eq}}\right)}{F\Gamma_{\text{RedH}}}\right| = \left|\frac{j_{\text{cath}}\left(E_{\text{pH}}^{\text{eq}}\right)}{F\Gamma_{\text{Ox}}}\right| \quad \text{[S40]}$$

Following **Equation [S40]** at potentials where $E = E_{\text{pH}}^{\text{eq}}$, both **Equations [S39]** collapse to the simple expression:

$$\boldsymbol{k_{\text{app}}(\text{pH}) = k_{\text{a}}^{0}10^{-(1-\alpha_{\text{a}})\text{pH}} + k_{\text{b}}^{0}10^{\alpha_{\text{b}}(\text{pH}-\text{p}K_{\text{w}})}} \quad \text{[S41]}$$

Equation [S41] is the final expression for the dependence of the apparent rate constant for I-PCET as a function of pH and is the same as **Main Text Equation [11]**.

1.3 Supplementary Note 3: Treatment of uncompensated internal resistance (R_u)

While in treating uncompensated internal resistance (R_u) using Ohm's law alone may lead to errors in peak position, we note here that, in our work, this possible source of error is likely to be quite minor. Residual uncompensated R_u never exceeded 1 Ω; as a result, CVs that passed less than 1 mA of current would experience at most a 1 mV error in potential positions. Given the intentionally small active surface area of our electrodes, currents near 1 mA were maintained through scan rates as fast as 100 V s^{-1} (see **Supplementary Section 1.1**). Trumpet plots collected between pH 4 and 13 fit either zero or very few points beyond this scan rate. For CVs with scan rates beyond 100 V s^{-1}, with currents on the order of 10 mA would result in *at most* a 10 mV error in peak position due to any possible error in accounting for 1 Ω residual R_u. This level of error is relatively minor and would be readily apparent as a linear skewing of both the anodic and cathodic traces of the trumpet plot away from ideal values. Additionally, the good agreement of the trumpet plot working curve fits for scan rates below and above 100 V s^{-1} indicate that residual R_u compensation is unlikely to be a major source of error.

1.4 Supplementary Note 4: Insensitivity of extracted k_{app} values to variation in fit charge transfer coefficient (α) values

The analysis of the Main Text invokes a simple exponential rate-driving force relationships for I-PCET with a potential-independent transfer coefficient. This treatment is mathematically identical to both Butler-Volmer formalisms for OSET as well as the Brønsted catalysis law for pure PT, and is sufficient to capture the pH-dependent trends in the data. The more complex Marcus-Hush-Chidsey[5] formalisms developed for outer-sphere surface ET reactions would predict a potential-dependent transfer coefficient at overpotentials that approach the reorganizational energy of the reaction. From pH 0 to pH 10, our data samples a 0.65 V overpotential range for the rate-limiting CPET step with hydronium as the donor; and from pH 10 to pH 14, our data samples a 0.21 V overpotential range for the rate-limiting reverse CPET with hydroxide as the acceptor. Thus, provided that I-PCET at GC-COOH can be described by even a modest reorganization energy (~1.5 eV),[6] the data simply do not sample an overpotential region where the two models can be distinguished, suggesting that a relatively simple exponential rate-driving force relationship akin to Butler-Volmer or Brønsted formalisms may be sufficient for modeling I-PCET in aqueous media for many systems.

In the remainder of this section we will show that the values of k_{app} extracted from trumpet plots are not sensitive to whether charge transfer coefficients used in trumpet plot simulations are fixed or used as fitting parameters. In this work charge transfer coefficients are utilized to make two different types of data fits, 1) a fit of simulated trumpet plots to experimental data (called α_{TP} here) and 2) a fit of the overall k_{app} vs pH slopes ($1-\alpha_a$ and α_b) in the caldera plot of **Main Text Figure 6** using **Main Text Equation [11]**. These values in theory refer to the same physical phenomena, however fits of data using the two methods above return different values for α. In the simulated trumpet plot working curves, the value of α_{TP} was used as a fitting parameter to simulate CVs and extract the k_{app} values referred to in the Main Text. Best fit working curves generally returned α_{TP} values of ~0.5, with a degree of variability even among pH replicates. Given that the trumpet plots at most pH conditions refer exclusively to I-PCET of either the hydronium-donor or water-donor I-PCET at GC-COOH, the α_{TP} values extracted for the low pH trumpet plots in theory refer to α_a and for the high pH to α_b. Our analysis then uses the k_{app} values extracted from trumpet plots to plot the pH dependence of k_{app}. From the k_{app} vs pH we assert that we can extract meaningful α_a and α_b values and use the values to make mechanistic claims about I-PCET at GC-COOH and I-PCET in general. The α_a and α_b values extracted from the slopes of $\log(k_{app})$ vs pH return values of 0.66 and 0.70 respectively. However, unlike the trumpet plot fitting using α_{TP}, α_a and α_b fit well across the entire applicable pH regimes.

To assess whether errors or uncertainty in fitting α_{TP} led to error in extracted k_{app} values, we calculated k_{app} values when α_{TP} was fixed. Using an analogous MATLAB script as was used to freely fit α_{TP}, trumpet plots were simulated using α_{TP} values constrained to 0.35, 0.5, and 0.65. In doing this, our goal was to see if these highly disparate α_{TP} values led to significant differences in k_{app} values determined for a given data set. **Supplementary Figure 4** shows the trumpet plot for the same pH 14 data in **Main Text Figure 4a** and **Supplementary Figure 12**, below, fit with explicitly defined charge transfer coefficients. The three trumpet plots allowed k_{app} and the E_{float} to be fit while α_{TP} was fixed to 0.35, 0.5 and 0.65 for the left, middle, and right panels respectively. In **Supplementary Figure 4** the red circles convey the same experimental peak potentials whereas the black diamonds represent the simulated $|E_{peak} - E^{eq}|$ for each scan rate for the defined α_{TP} and fit k_{app} and E_{float} values. From **Supplementary Figure 12** it is apparent that major deviations in experimental peak positions and calculated peak positions are significant only at the three of four fastest scan rates, that is where $|E_{peak} - E^{eq}|$ is greater than about 70 mV. Most trumpet plots in this work likewise only fit a small number of points with this significant of a peak separation. Allowing α_{TP} to fit freely for this data set returned a value of 0.74 and k_{app} = 4,300 s^{-1}. The fixed α_{TP} values returned k_{app} values of 5,200 s^{-1} for α_{TP} = 0.35, 4,600 s^{-1} for α_{TP} = 0.5, and 4,300 s^{-1} for α_{TP} = 0.65. The 20% variation seen across this wide range of fixed α_{TP} values corresponds to shifts of only 0.08 log units, a deflection that would be visually indistinguishable on the caldera plot shows in **Main Text Figure 5**. The small deviation among in k_{app} makes sense given that differences in this value represent a horizontal shift of the trumpet plot (see **Supplementary Section 1.6** for equations relating k_{app} to scan rate). Though α_{TP} affects the relative shape of the simulated trumpet plots, it has little effect at the scan rate range where $|E_{peak} - E^{eq}|$ becomes significant, and thus the position trumpet plot's opening.

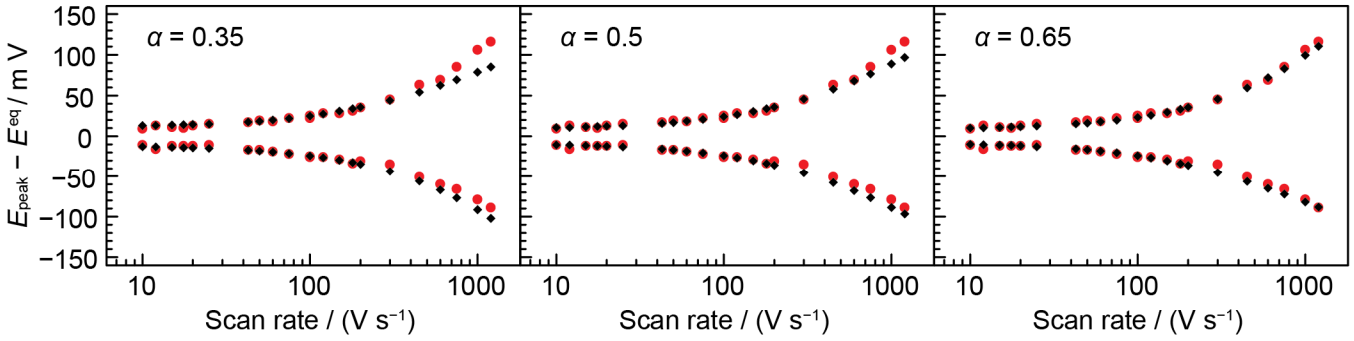

Supplementary Figure 4: Comparison of trumpet plots fit for fixed charge transfer coefficients for the same pH 14 trumpet plot data. Red circles convey experimental data while black diamonds are the fits for the different α_{TP} values quoted in the above frames. Similar discrepancies are seen in the experimental vs fit $E_p - E^{eq}$ data between the three fit conditions until a scan rate of around 600 V s^{-1}. Beyond this scan rate, the $\alpha_{TP} = 0.65$ data clearly fit much better. Despite the difference in these high scan rate fits, the extracted k_{app} values differ by only 0.08 log units between α_{TP} values.

To further confirm that errors in the fit α_{TP} values did not lead to errors in the k_a^0, k_b^0, α_a, and α_b values extracted from the caldera plot, we fit simulated trumpet plots with three fixed α_{TP} values at all pH values. A comparison of caldera plots of k_{app} vs pH data when α_{TP} was allowed to be fit or was fixed appears in **Supplementary Figure 5**. The values represented in gray squares in **Supplementary Figure 5** are identical to the k_{app} vs pH data in **Main Text Figures 5 and 6**. Values extracted when α_{TP} was constrained to 0.35 (green downward triangle), 0.5 (blue upward triangle), and 0.65 (red circle) overlay the fit-α_{TP} k_{app} values, appearing nearly indistinguishable from one another. The lack of k_{app} dependence on the α_{TP} used to fit trumpet plots is shown numerically in **Supplementary Table 1** which relays values for k_a^0, k_b^0, α_a, and α_b determined by fitting **Main Text Equation [11]** to the caldera plots in **Supplementary Figure 5**. All four values are internally nearly identical between the four fitting conditions. As charge transfer coefficients reflect how a perturbation from equilibrium affects the kinetics of a reaction, it follows that the α_a and α_b values which span multiple pH units and therefore several hundred millivolts of driving force are far more reliable that the α_{TP} values which are extracted from the legs of trumpet plots that span only a few dozen millivolts. The consistency of the data in **Supplementary Table 1** show that the k_a^0, k_b^0, α_a, and α_b values extracted from the caldera plot data in **Main Text Figures 5 and 6** and used in our analysis are robust parameters, agnostic to the α_{TP} value used to extract k_{app} values from trumpet plots and make the caldera plot.

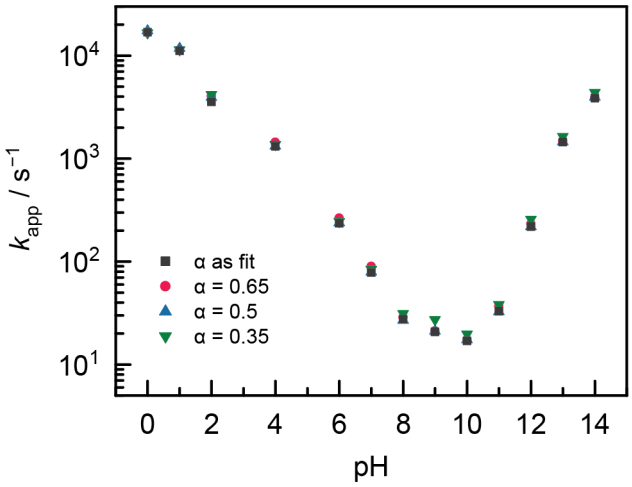

Supplementary Figure 5: Comparing the effect on the overall caldera plot of allowing α values to vary in each trumpet plot fitting versus fixing the α values to a range of possible values. The caldera plot calculated when α_{TP} was fit is shown in gray squares, and when α_{TP} was constrained to 0.35 is shown in green downward triangles, 0.5 in blue upward triangles, and 0.65 in red circles.

Supplementary Table 1: Comparison of extracted caldera plot parameters k_a^0, k_b^0, α_a, and α_b when the trumpet plot α_{TP} is fit or fixed.

trumpet plot fitting α_{TP}	parameters extracted from caldera plots					
	k_a^0 (s^{-1})		k_b^0 (s^{-1})		α_a	α_b
as fit	20890	$= 10^{4.3}$	5032	$= 10^{3.7}$	0.658	0.703
0.35	21170	$= 10^{4.3}$	5701	$= 10^{3.8}$	0.666	0.699
0.50	22160	$= 10^{4.3}$	5126	$= 10^{3.7}$	0.656	0.705
0.65	22070	$= 10^{4.3}$	5115	$= 10^{3.7}$	0.656	0.697

1.5 Supplementary Note 5: Repercussions of observed super-Nernstian scaling

A 64 mV pH^{-1} scaling in equilibrium potential is observed for I-PCET at GC-COOH, yet we employ a "truly-Nernstian" 59 mV pH^{-1} scaling to derive the caldera model. This difference amounts to a total deviation of 70 mV or 1.6 kcal $mole^{-1}$, a relatively small amount when considering this effect occurs over fourteen orders of magnitude in proton donor/acceptor concentrations. In our study we independently measure observed I-PCET rate constants at a given pH and the corresponding equilibrium potentials of I-PCET at each pH. Thus our data provide a direct measurement of the scaling of rate with pH and rate with potential, irrespective of the scaling of pH and potential. In the limit that the pH/potential scaling is exactly Nernstian, a common transfer coefficient describes how rate scales with potential and how rate scale with pH, each for both the acid and base reactions. In accounting for a slight deviation away from the ideal Nernstian slope, the linear free energy parameter describing the *E*-dependence, α_E, and the linear free energy parameter describing the pH-dependence, α_{pH} are not exactly the same. However, since we measure the equilibrium potential *E* and the pH independently for all experiments, we can isolate the two values, even in the limit of the slight deviation away from pure Nernstian scaling. The α values reported in the main text are authentic α_{pH} values of 0.66 for the acid and 0.70 for the base reactions. The non-Nernstian scaling of α_E can be accounted for by plotting the apparent rate constant at the independently measured equilibrium potential for each pH. The electrochemical transfer coefficients for the acid and base reactions, $\alpha_{E,acid}$ and $\alpha_{E,base}$, relate to the slopes of the $\log(k_{app})$ vs *E* dependence at potentials where the acid and base reaction are each dominant λ_{acid} (pH 0 to 9) and λ_{base} (pH 11 to 14) by the following relation:

$$1 - \alpha_{E,\mathrm{acid}} = \lambda_{\mathrm{acid}} \times \frac{\ln(10)RT}{F} \quad \text{[S42a]}$$

$$\alpha_{E,\mathrm{base}} = \lambda_{\mathrm{base}} \times \frac{\ln(10)RT}{F} \quad \text{[S42b]}$$

Where *R* and *F* represent their usual meaning and *T* represents room temperature. **Supplementary Figure 6** plots k_{app} for each pH with an ideal 59 mV pH^{-1} scaling on the left caldera plot as in **Main Text Figure 5** and the observed 64 mV pH^{-1} on the right caldera plot. In each caldera plot, the bottom x-axis represents potential and the top x-axis represents the pH where each rate is measured. Each kinetic measurement is mapped from the pH value on the top axis to and equilibrium potential value on the bottom x-axis with either a 59 mV pH^{-1} (left) or 64 mV pH^{-1} (right) scaling. As expected, the slopes of the left plot return α_E values of 0.66 for the acid and 0.70 for the base reaction, identical to the corresponding α_{pH} values, as expected mathematically. Upon accounting for the slight super-Nernstian behavior (right plot), we recover α_E transfer coefficients of 0.68 for the acid reaction and 0.65 for the base reaction. The differences in these values are small, ~8% and ~4% respectively, and, thus have no substantial impact any of the overall conclusions.

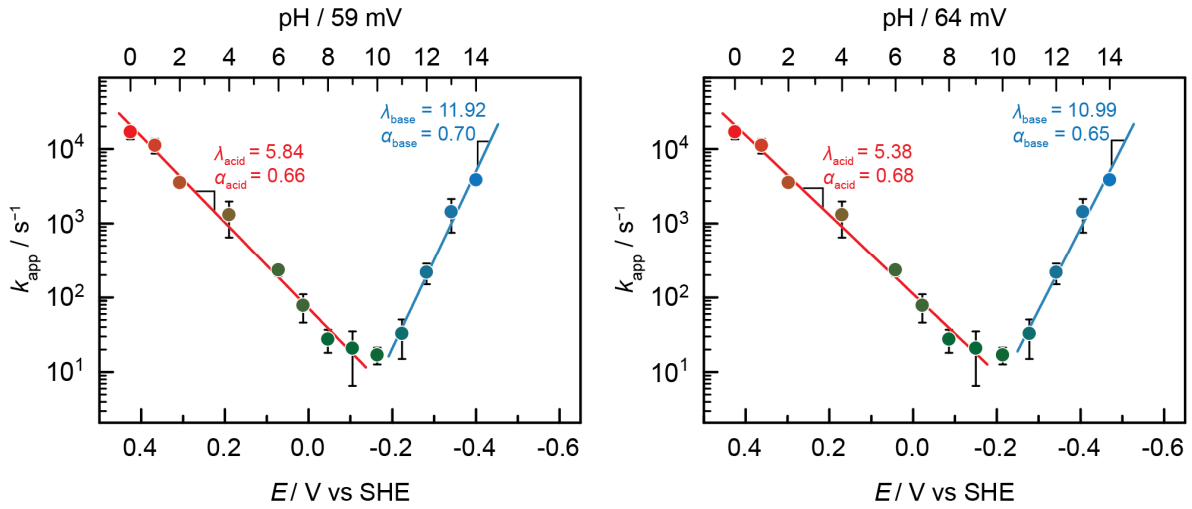

Supplementary Figure 6: Caldera plots of the k_{app} vs pH data in **Main Text Figure 5** plotted as a function of pH (top x-axis) and potential (bottom x-axis), In the left caldera plots, the kinetic data at each pH marked on the top axis is mapped to an equilibrium potential value using an ideal Nernstian scaling, while the right caldera plot maps each pH to equilibrium potential using the measured 64 mV pH^{-1} scaling. These plots illustrate how the λ values in **Equations [S42a]** can be used to determine $\alpha_{E,acid}$ and $\alpha_{E,base}$ values for each E vs pH scaling. (Triplicate data is mean of three trials, error bars = 1σ)

Given the small degree of non-ideality in the pH/potential scaling, 70 mV over 14 pH units, we refrain from speculating about its origin. Indeed, slight deviations from Nernstian scaling are commonly observed for homogenous[7] and interfacial I-PCET processes[8] on the order of ~4 mV pH^{-1} without considerable comment. We can, however, rule out a number of potential sources of super-Nernstian behavior. As I-PCET at GC-COOH occurs at a well-defined site that resides within the electrochemical double layer,[9] a grossly imbalanced electron/proton stoichiometry can be excluded (i.e. exchange of one proton at this interface is expected to correspond to compensatory flow of a single electron from the external circuit). Furthermore, it is unlikely that the supernumerary 5 mV pH^{-1} deviation arises from a cation-related effect as the equilibrium potential for I-PCET at GC-COOH is constant across 1 M LiOH, NaOH, KOH, and CsOH electrolyte. While super-Nernstian shifts of >70 mV pH^{-1} has been invoked to result from a mixed potential arising from multiple active site structures or electroactive phases as in IrO_2 hydrates,[10] this explanation cannot apply to the molecularly well-defined GC-COOH active sites. Whatever the origin of this non-ideality, we reiterate that this 5 mV pH^{-1} deviation minimally impacts the core findings of this work.

1.6 Supplementary Note 6: Insensitivity of extracted k_{app} values to variation in fit of E_{float} values

In this section we will show the values of k_{app} extracted from trumpet plots are not sensitive to the E_{float} values used to fit the trumpet plots. In regards to the fitting of the E_{float}, we stress that this $E_p - E^{eq}$ splitting is routinely treated as a constant offset, equal for all scan rates (v) in a given trumpet plot.[11,12] In this study, E_{float} values were generally fit to values between 10 and 20 mV with a mean of 15 mV and a median of 14 mV. In order to ensure that errors in E_{float} do not lead to overall error in the caldera plot analysis, we compare the cases where E_{float} values were allowed to vary to the case where E_{float} values are set to 0 mV, 15 mV, and 30 mV for each trumpet plot. As forcing E_{float} values to equal certain values would cause large errors and make the working curves in our fitting algorithm impossible to fit, we instead consider how a constant offset in the potential terms ($E_p - E^{eq}$) for an analytical expression for k_{app} would affect resulting k_{app} values.

The following analysis is based on the original method of Laviron,[13] where only the highly irreversible linearized $E_p - E^{eq}$ vs log(v) portion on the trumpet plot is fit to two equations, one for the anodic and one for the cathodic part of the trumpet's opening. These equations apply only in this regime where a surface confined ET process is fully electrochemically irreversible and kinetically controlled.

$$E_{p,a} - E^{eq} = -\frac{\ln(10)RT}{(1-\alpha)F}\log\left(\frac{RT}{(1-\alpha)F}\times\frac{k_{app}}{v}\right) + E_{float} \quad [S43a]$$

$$E_{p,c} - E^{eq} = \frac{\ln(10)RT}{\alpha F}\log\left(\frac{RT}{\alpha F}\times\frac{k_{app}}{v}\right) - E_{float} \quad [S43b]$$

Where $E_{p,a}$ and $E_{p,c}$ are the peak potentials for the anodic and cathodic traces of the trumpet plot. E_{float} is the potential separation of the $E_{p,a}$ and $E_{p,c}$ from E^{eq} when the surface reactions is highly reversible at low scan rates. This term is not included in Laviron's initial assessment of trumpet plots and its use as a fitting parameter is what we are considering in this section.

Equations [S43] can be distributed into the product of three terms, i) a scaling term including α, ii) a k_{app} term, and iii) a scan rate term:

$$\left(E_{p,a} - E^{eq}\right) - E_{float} = -\frac{\ln(10)RT}{(1-\alpha)F}\log\left(\frac{RT}{(1-\alpha)F}\right) - \frac{\ln(10)RT}{(1-\alpha)F}\log\left(k_{app}\right) + \frac{\ln(10)RT}{(1-\alpha)F}\log(v) \quad [S44a]$$

$$\left(E_{p,c} - E^{eq}\right) + E_{float} = \frac{\ln(10)RT}{\alpha F}\log\left(\frac{RT}{\alpha F}\right) + \frac{\ln(10)RT}{\alpha F}\log\left(k_{app}\right) - \frac{\ln(10)RT}{\alpha F}\log(v) \quad [S44b]$$

In regards to the peak potential for a given scan rate, a change in the E_{float} value from the true value of $E_p - E^{eq}$ will have an effect on k_{app} of the working curve. For a given condition, we can posit a supposed "real" apparent rate constant ($k_{app,real}$), that is the true value of k_{app} that a supposed error in our E_{float} would fail to capture. The irreversible portion of a trumpet plot with a $k_{app,real}$ would bear the same functional form as **Equations [S44]** a real value for E_{float}, $E_{float,real}$. At the condition where E_{float} is completely erroneously applied $E_{float,real} = 0$:

$$\left(E_{p,a} - E^{eq}\right) - E_{float,real} = -\frac{\ln(10)RT}{(1-\alpha)F}\log\left(\frac{RT}{(1-\alpha)F}\right) - \frac{\ln(10)RT}{(1-\alpha)F}\log\left(k_{app,real}\right) + \frac{\ln(10)RT}{(1-\alpha)F}\log(v) \quad [S45a]$$

$$\left(E_{p,c} - E^{eq}\right) + E_{float,real} = \frac{\ln(10)RT}{\alpha F}\log\left(\frac{RT}{\alpha F}\right) + \frac{\ln(10)RT}{\alpha F}\log\left(k_{app,real}\right) - \frac{\ln(10)RT}{\alpha F}\log(v) \quad [S44b]$$

Subtracting **Equation [S45a]** from **Equation [S44a]** and **Equation [S45b]** from **Equation [S44b]** allows quantification of the resultant error in measurements of k_{app} from $k_{app,real}$ due to an error in a fit E_{float} value:

(anodic:) $$E_{float} - E_{float,real} = \Delta E_{float} = \frac{\ln(10)RT}{(1-\alpha)F}\log\left(\frac{k_{app,real}}{k_{app}}\right) \quad [S46a]$$

(cathodic:) $$E_{float} - E_{float,real} = \Delta E_{float} = \frac{\ln(10)RT}{\alpha F}\log\left(\frac{k_{app,real}}{k_{app}}\right) \quad [S46b]$$

Where **Equation [S46a]** refers to an error in the anodic peaks and **Equation [S46b]** an error in the cathodic peaks. As an example, in the case where $\alpha = 0.5$ an error in E_{float} of 0.015 V would result in an error of $\log(k_{app,real}/k_{app})$ equal to 0.127 log units or a factor of 40 % on a linear scale. On a logarithmic scale such as is seen in **Main Text Figures 5 and 6** and **Supplementary Figure 7,** below, a shift of 0.127 is a rather modest error. **Supplementary Figure 7** depicts four caldera plots, one where the E_{float} was fit and three where the extracted k_{app} values are modified to supposed $k_{app,real}$ values. In the three modified caldera plots, each trumpet plot in the data set was modified such that for a given k_{app} with a fit E_{float} value, a $k_{app,real}$ was calculated using **Equations [S46]** for several defined E_{float} value. The three fixed E_{float} caldera plots were calculated for cases where E_{float} equaled 0 mV, 15 mV, and 30 mV. From the figure it is clear that the overall caldera plot shape is simply a log-linear offset between E_{float} values. A comparison of the plots with fixed E_{float} values of 0 mV and 30 mV highlights that even an error of 30 mV in fit E_{float} would have a negligible effect on the analysis in the main text. Furthermore, even if the variability in our measured E_{float} values was not consistent between our pH values, but varied up to 30 mV, a comparison of the green triangles and red circles suggests that this large perturbation would result in nearly identical caldera shaped profiles. The nearly perfect overlay of the blue triangles and gray squares in **Supplementary Figure 7** also suggests that a E_{float} of 15 mV is likely the "true" $E_{peak} - E^{eq}$ value in the reversible limit for GC-COOH I-PCET. **Supplementary Table 2** contains the k_a^0, k_b^0, α_a, and α_b values extracted from each of these caldera plots, quantifying that a systemic error in E_{float} has almost no effect on the extracted parameters central to the claims of the main text.

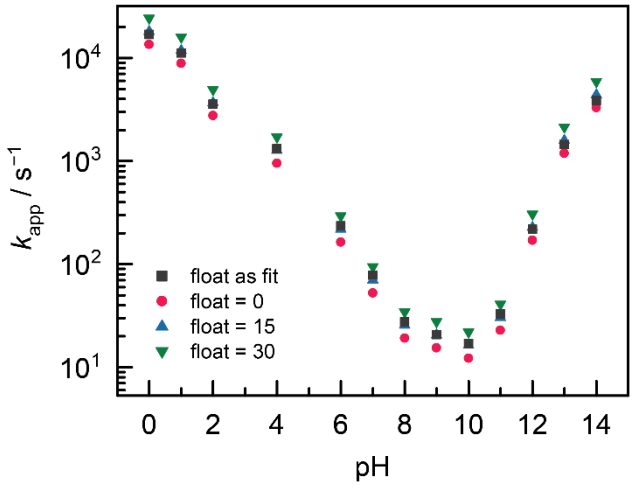

Supplementary Figure 7: Comparing the effect on the overall caldera plot of allowing E_{float} values to vary in each trumpet plot fitting versus fixing the E_{float} values to a range of possible values. The caldera plot calculated when E_{float} was fit is shown in gray squares and when E_{float} constrained to 0 mV is shown in green downward triangles, 15 mV in blue upward triangles, and 30 mV in red circles.

Supplementary Table 2: Comparison of extracted caldera plot parameters k_a^0, k_b^0, α_a, and α_b when the trumpet plot E_{float} is fit or fixed.

trumpet plot fitting E_{float} (V)	parameters extracted from caldera plots			
	k_a^0 (s^{-1})	k_b^0 (s^{-1})	α_a	α_a
as fit	20,890 $= 10^{4.3}$	5,032 $= 10^{3.7}$	0.659	0.703
0.000	16,480 $= 10^{4.2}$	4,292 $= 10^{3.6}$	0.652	0.725
0.015	22,040 $= 10^{4.3}$	5,760 $= 10^{3.8}$	0.653	0.726
0.030	29,540 $= 10^{4.5}$	7,686 $= 10^{3.9}$	0.652	0.724

1.7 Supplementary Note 7: A note on peak fitting and baselining protocol

In this work, peak positions for the cathodic and anodic traces of the GC-COOH carboxylate I-PCET reflect the potentials with maximal or minimal current relative to simple linear baselines. These linear baselines were defined by the inflection points on either side of the carboxylate's anodic and cathodic peaks (**Supplementary Figure 8**, left). We chose to fit CV baselines based solely on the carboxylate peak currents, because, while the carboxylate peaks were consistent and well behaved, they overlapped with the pyrazine PCET peaks. Rigorous fitting of a Gaussian peak to the carboxylate I-PCET peak would therefore necessitate fitting two Gaussians to the overlapping pyrazine I-PCET currents as well. In order to do so, a reliable baselining method across the entire potential span of these three peaks would be needed, however no such analytical or experimental baselining procedure could be found. To corroborate our use of a simple carboxylate-only linear baseline for the carboxylate peak, we compared the simple baselining procedure we used to a three-component fit on one of the very few collected trumpet plot data sets were a linear baseline across all three PCET peaks returned reliable fits. **Supplementary Figure 8** displays four cyclic voltammograms in two columns from a trumpet plot collected at pH 8, with scan rates of 0.01 V s^{-1}, 0.1 V s^{-1}, 1 V s^{-1}, and 10 V s^{-1} spanning the fully reversible and irreversible trumpet plot regimes. The left column of CVs utilizes the simple linear baselining, while the right column displays the three component fit of the same CVs, with two Gaussian peaks corresponding to PCET at the pyrazines (gray) one for the carboxylate (dark blue) and a fit linear baseline that spans all three peaks (orange). In this method peaks were constrained to minimize the difference in the total sum of the fit currents (light blue) and the raw current (black) *and* to minimize the difference in area between the three Gaussian peaks on the anodic trace and cathodic trace to reflect the equal surface concentration of each I-PCET active site.

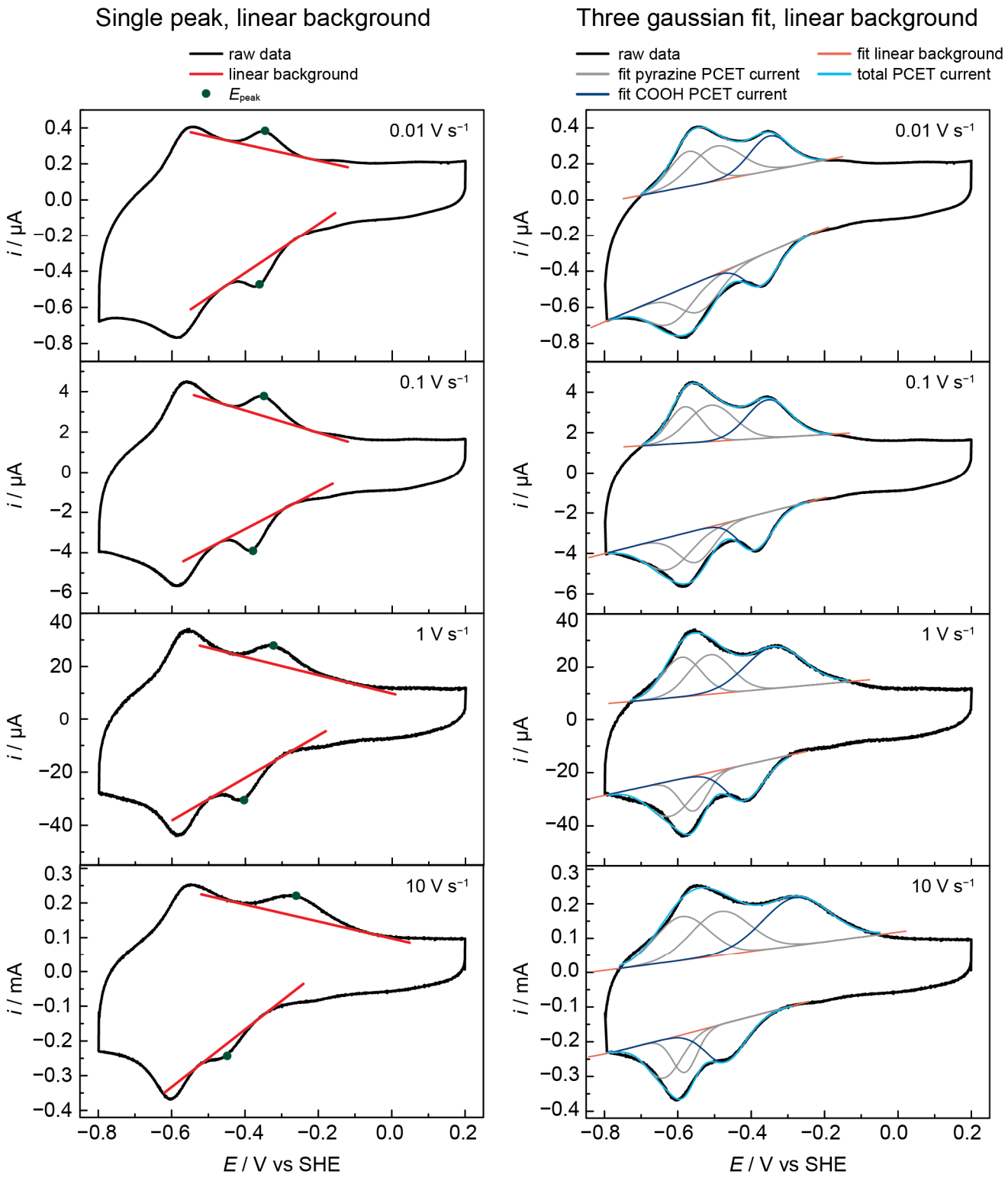

Supplementary Figure 8: Comparison of peaks fits for the generally utilized simple, inflection-point-based baselining procedure (left) and three component Gaussian procedure (right). The right and left columns show the same CVs at four different scan rates, each an order of magnitude apart representative of the full reversible to irreversible regime. Note the quality of the numerically fit linear baseline in the right-hand column to the more complex underlying currents in the cyclic voltammograms in **Supplementary Section 2.1** below.

The two fitting procedures return trumpet plots that are nearly identical expect for minor variations in E^{eq} and E_{float}, neither of which impact the rate constant fitting algorithm used. The raw peak positions extracted from both fitting procedures are shown in **Supplementary Figure 9**, left, and the data are reproduced in on the right with adjustment for the variations in E^{eq} and E_{float}. Upon accounting for these minor adjustments, 6 mV for E^{eq} and 4 mV for E_{float}, the trumpet plots overlay (**Supplementary Figure 9**, right). From these plots it is readily apparent that the absolute values of the $E_{peak} - E^{eq}$ are essentially unaffected by the baseline fitting procedure. Fitting these trumpet plots with these two baselining methods extracts apparent rate constants of 35 s^{-1} using the simple baselining procedure (red) and 38 s^{-1} using the three-component procedure (blue), an insignificant difference on a logarithmic scale. While the more rigorous three-component method was not suitable for all the collected data, its nearly exact agreement with the simple baselining procedure in this data set corroborates the use of the simple, inflection-point-defined linear baselining method in this work.

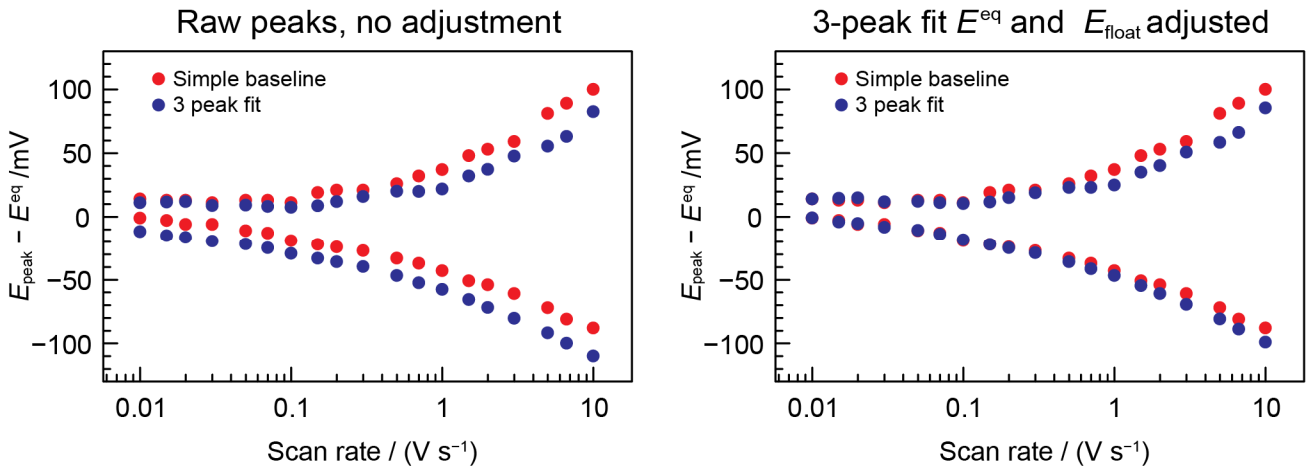

Supplementary Figure 9: Overlay of trumpet plots using two baselining methods, a simple inflection-point-defined linear baseline (red) and a three-peak fit linear baseline (blue). The left overlay depicts the raw extracted peak values, while the right overlay adjusts for variation in E^{eq} and E_{float} found for each fitting method. In the both panels it is apparent that the baselining procures have little effect on the $E_{peak} - E^{eq}$ values found for each scan rate.

1.8 Supplementary Note 8: A note on the isolation of peak potentials for I-PCET at GC-COOH and the protonation of the pyrazine linker during carboxylate I-PCET

As the peaks corresponding to I-PCET at the carboxylic acid partially overlap with the peaks for I-PCET at the nitrogen atoms of the pyrazine linker of GC-COOH, it is essential to ensure that differential protonation of pyrazinic nitrogen sites at different scan rates did not introduce convolutions in our kinetic interpretation. The three-Gaussian CV fits described in **Supplementary Note 7** and shown in **Supplementary Figure 8** allow quantification of the charge passed and corresponding protonation of each individual site for a given potential. In **Supplementary Figure 8** the potentials corresponding to the maximum (on the anodic trace) and minimum (on the cathodic trace) of the dark blue Gaussian curves correspond to $E_{p,a}$ and $E_{p,c}$ of I-PCET at GC-COOH respectively. First, looking at the cathodic trace, as the potential is scanned, negatively the more basic carboxylic acid site is protonated first leading to a peak maximum at $E_{p,c}$. Here no current corresponding to the pyrazine peaks has flowed. Similarly, on the anodic trace, starting from the lowest potential all three peaks are protonated. Scanning to positive potentials deprotonates the pyrazine peaks first, and by the time the potential corresponding to the maximum of the carboxylic I-PCET peak, $E_{p,a}$, is reached, the pyrazines have been completely deprotonated and the only reaction occurring at this potential is the deprotonation of the carboxylate. Separating the currents for the I-PCET currents at the three sites in this way shows that at $E_{p,a}$ and $E_{p,c}$ the potentials pertinent to the trumpet plot analysis, only current due to the carboxylate I-PCET flows. It is apparent from comparing the CVs in the right-hand column of **Supplementary Figure 8** that, even though the positions of the peaks shift as a function of scan rate, the isolation of the carboxylic acid peak potentials from the pyrazine current is maintained at every scan rate. The foregoing analysis highlights that, at $E_{p,a}$ and $E_{p,c}$, the protonation of the pyrazine linker, and therefore the nature of the electronic communication between the I-PCET active carboxylic sites and the bulk electrode is consistent across the entire investigated scan rate range. As a result, it is highly unlikely that variation in the linker chemistry as function of scan rate resulted in errors in measured carboxylate peak positions or convolutions in the fitting of trumpet plot data in our analysis.

2. Supplementary Data

2.1 Supplementary Data 1: Reversible cyclic voltammogram from each pH at 100 mV s^{-1}

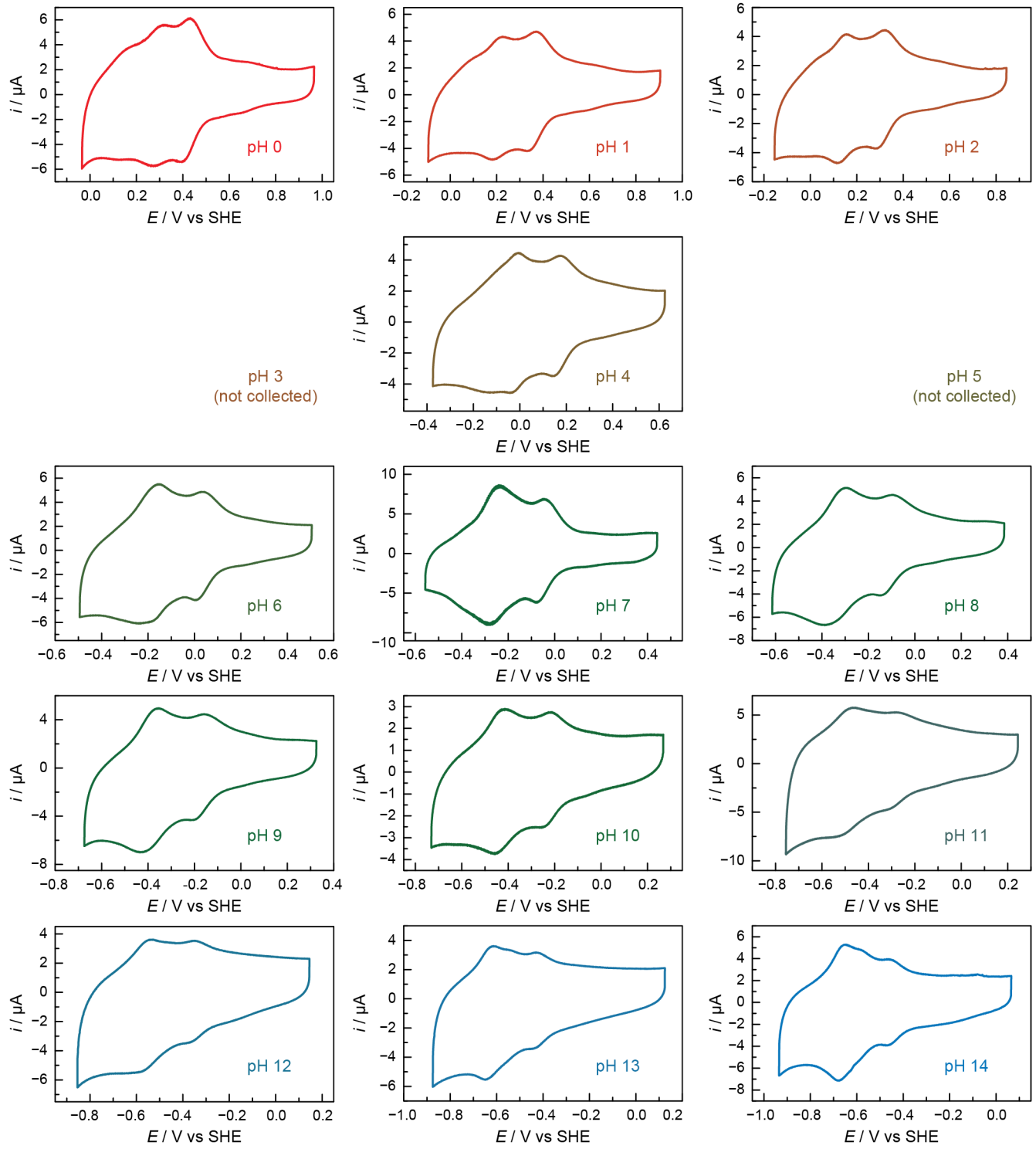

Supplementary Figure 10: Cyclic voltammograms from each pH at 100 mV s^{-1}, a scan rate for which I-PCET at GC-COOH is reversible at every pH (see trumpet plots in **Supplementary Figure 12**) Each CV is plotted against the standard hydrogen electrode reference (SHE) Slight variation in underlying pseudo-capacitive current and relative coverage of GC-COOH are apparent between electrodes, however the positions and prominence of the more positive peak corresponding to I-PCET at the carboxylic acid near (0.4 vs RHE) is maintained under all conditions. Note the variability of the more negative I-PCET peaks corresponding to I-PCET the surface pyrazine nitrogen atoms (near 0.2 vs RHE). Data were not collected for pH 3 and pH 5.

2.2 Supplementary Data 2: Representative cyclic voltammograms at pH 0, pH 9, and pH 14

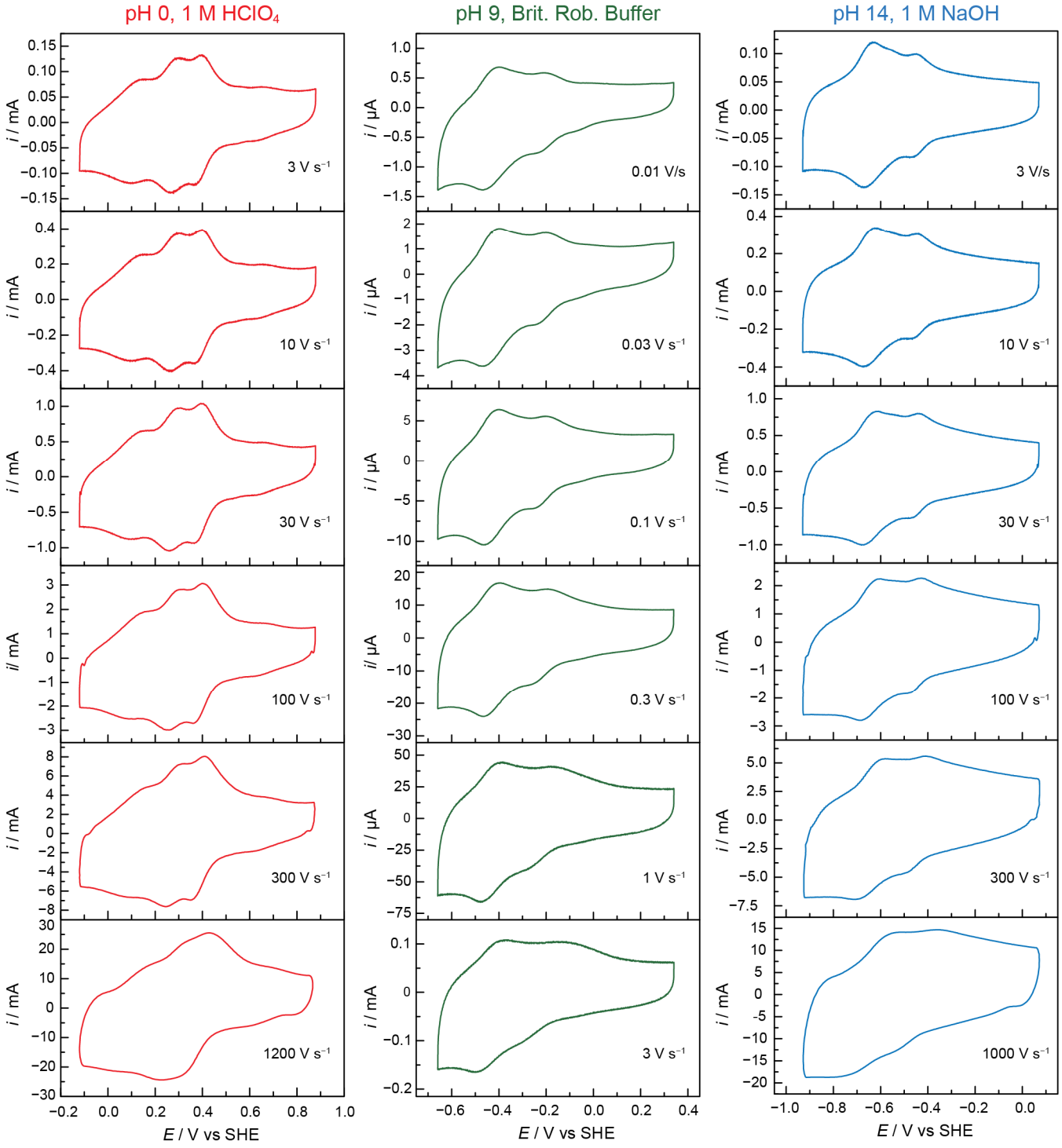

Supplementary Figure 11: Representative CVs from trumpet plots at pH 0, pH 9 and pH 14 at relevant scan rates that span the reversible and irreversible regimes. CVs are resistance compensated and plotted in reference to the standard hydrogen electrode (SHE). All CVs for a given pH group are from the same electrode. The peaks corresponding to I-PCET at the surface carboxylate are found near +0.4 V for pH 0, –0.2 V for pH 9, and –0.4 V for pH 14. Note the vastly dissimilar scan rates where peaks begin to diverge between the fastest pH values (pH 0 and pH 14) and the slowest (pH 9)

2.3 Supplementary Data 3: Representative trumpet plots from all 13 pH values

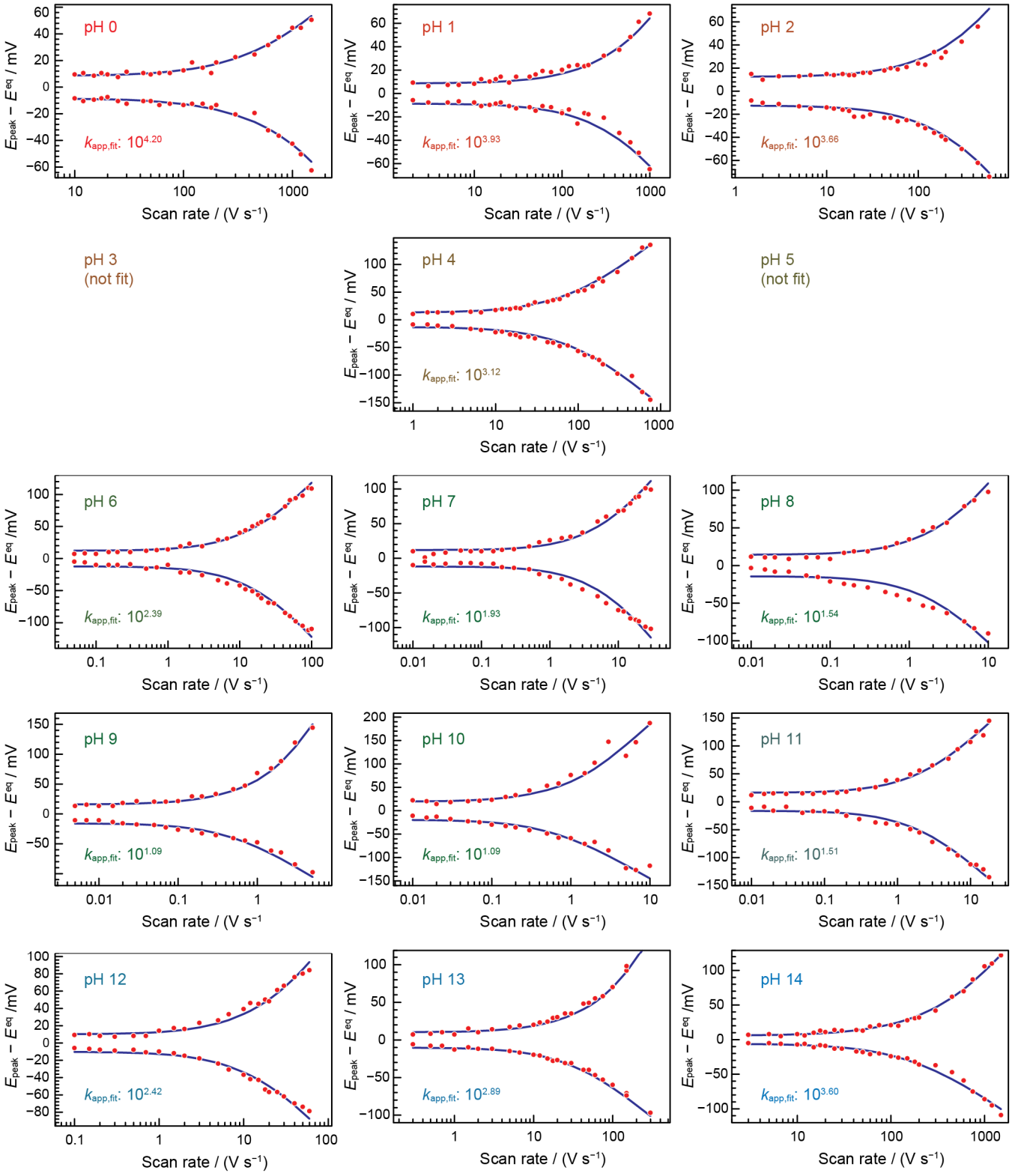

Supplementary Figure 12: One representative trumpet plot of triplicated data for each pH. Red circles represent peak positions and purple lines represent data fits. Note the vast differences scale for the in logarithmic x-axis representing scan rate. Each trumpet plot displays the fit k_{app} value for that data set. Data were not collected for pH 3 and pH 5.

2.4 Supplementary Data 4: Dependence of k_{app} on buffer concentration

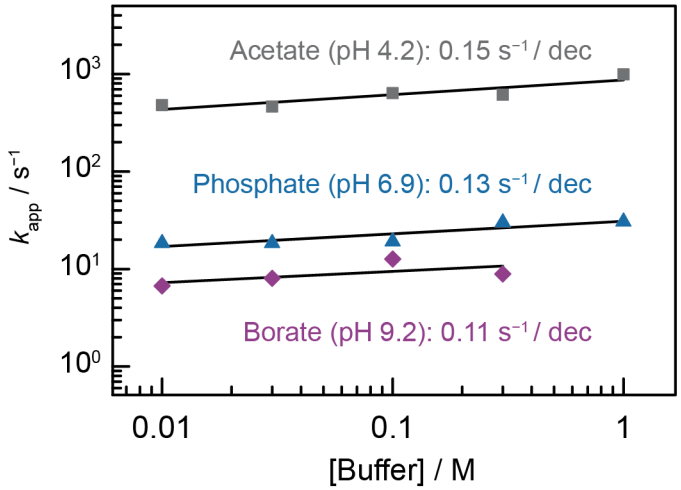

Supplementary Figure 13: Individual dependence of I-PCET at GC-COOH on the concentration of each buffer species alone at the pH corresponding to the buffers pK_a (pK_{a2} for phosphate). All data were collected in 1 M total ionic strength, supplemented with $NaClO_4$. The data show negligible dependence of I-PCET rate constant (k_{app}) on each buffer, especially compared to the concentration of hydronium and hydroxide (pH). This indicates the buffers serve only to control overall H_3O^+ and OH^- activities, but do not act effectively as donors or acceptors themselves.

2.5 Supplementary Data 5: Dependence of k_{app} on supporting cation identity

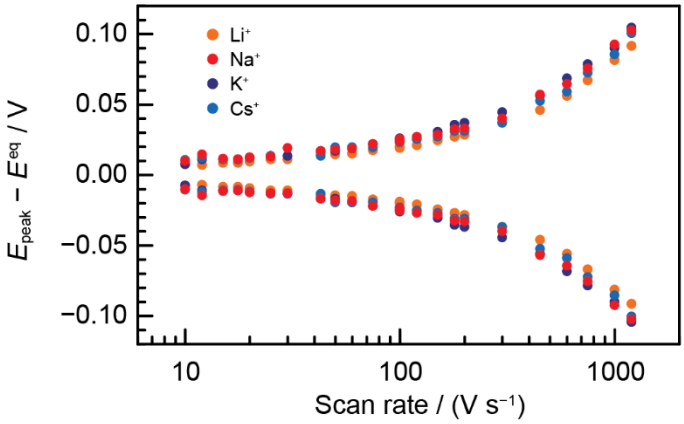

Supplementary Figure 14: Dependence of I-PCET for four different cations. To ensure the identity of the supporting cations did not affect I-PCET kinetics at GC-COOH, the rates of PCET for four alkali cations at pH 14 were compared.[14] Trumpet plots were collected for the same electrode at pH 14 in 1 M LiOH, NaOH, KOH, and CsOH. The data overlay nearly perfectly with k_{app} values of $10^{3.6}$ for NaOH and KOH and $10^{3.7}$ for LiOH and CsOH. These data indicate that this I-PCET reaction rate is agnostic of supporting cation and suggests there are no significant interactions between GC-COOH sites and the Na^+ supporting ions used in the central data of this study.

2.6 Supplementary Data 6: Images of electrode preparation

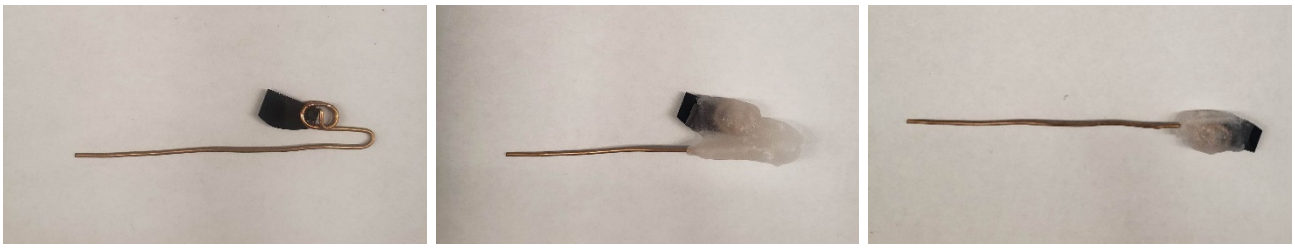

Supplementary Figure 15: Images of electrode preparation steps. Left: Functionalized glassy carbon electrode placed in the loop of a Cu wire and bonded with conductive paste. Middle: Electrode assembly after dipping in wax to seal Cu off from electrolyte. Cu wire was dipped into wax loop first to ensure Cu was sealed without wax contacting exposed glassy carbon. Right: Excess wax is removed and wire is straightened to complete electrode preparation. At no point during electrochemical analysis did the electrolyte rise above the insulating wax layer.

3. Supplementary References

1. Laviron, E. Theoretical study of a $1e^-$, $1H^+$ surface electrochemical reaction (four-member square scheme) when the protonation reactions are at equilibrium. *J. Electroanal. Chem. and Inter. Electrochem.* **109**, 57–67 (1980).
2. Finklea, H. O. & Haddox, R. M. Coupled electron/proton transfer of galvinol attached to SAMs on gold electrodes. *Phys. Chem. Chem. Phys.* **3**, 3431–3436 (2001).
3. Finklea, H. O. Theory of Coupled Electron–Proton Transfer with Potential-Dependent Transfer Coefficients for Redox Couples Attached to Electrodes. *J. Phys. Chem. B* **105**, 8685–8693 (2001).
4. Savéant, J. M. & Costentin, C. *Elements of Molecular and Biomolecular Electrochemistry: An Electrochemical Approach to Electron Transfer Chemistry*. (Wiley, 2019).
5. Chidsey, C. E. D. Free Energy and Temperature Dependence of Electron Transfer at the Metal-Electrolyte Interface. *Science* **251**, 919–922 (1991).
6. Zeng, Y., Smith, R. B., Bai, P. & Bazant, M. Z. Simple formula for Marcus–Hush–Chidsey kinetics. *Journal of Electroanalytical Chemistry* **735**, 77–83 (2014).
7. Agarwal, R. G. *et al.* Free Energies of Proton-Coupled Electron Transfer Reagents and Their Applications. *Chem. Rev.* **122**, 1–49 (2022).
8. Wise, C. F. & Mayer, J. M. Electrochemically Determined O–H Bond Dissociation Free Energies of NiO Electrodes Predict Proton-Coupled Electron Transfer Reactivity. *J. Am. Chem. Soc.* **141**, 14971–14975 (2019).
9. Warburton, R. E. *et al.* Interfacial Field-Driven Proton-Coupled Electron Transfer at Graphite-Conjugated Organic Acids. *J. Am. Chem. Soc.* **142**, 20855–20864 (2020).
10. Burke, L. D., Mulcahy, J. K. & Whelan, D. P. Preparation of an oxidized iridium electrode and the variation of its potential with pH. *J. Electroanal. Chem. and Inter. Electrochem*,**163**, 117–128 (1984).
11. Hirst, J. & Armstrong, F. A. Fast-Scan Cyclic Voltammetry of Protein Films on Pyrolytic Graphite Edge Electrodes: Characteristics of Electron Exchange. *Anal. Chem.* **70**, 5062–5071 (1998).
12. Armstrong, F. A. *et al.* Fast voltammetric studies of the kinetics and energetics of coupled electron-transfer reactions in proteins. *Faraday Disc.* **116**, 191–203 (2000).
13. Laviron, E. General expression of the linear potential sweep voltammogram in the case of diffusionless electrochemical systems. *Journal of Electroanalytical Chemistry and Interfacial Electrochemistry* **101**, 19–28 (1979).
14. Delley, M. F., Nichols, E. M. & Mayer, J. M. Electrolyte Cation Effects on Interfacial Acidity and Electric Fields. *J. Phys. Chem. C* **126**, 8477–8488 (2022).